Universitat d'Alacant
Universidad de Alicante

University of Alicante

Department of Applied Physics

Quantum Transport in Graphene Atomic-sized Contacts

Author:
Yelko del Castillo Hernández

Supervisors:
Dr. Joaquín Fernández Rossier
Dr. Carlos Sabater Piqueres

A thesis submitted in fulfilment of the requirements for the degree of Master of

Molecular Nanoscience and Nanotechnology

September 3, 2020

Contents

Chapter 1

Introduction

This master thesis is devoted to the theoretical study of electronic transport across atomic-sized constrictions in graphene. The motivation of this work is threefold. First, at the start of the project, we wanted to study the transport between two graphene electrodes that are non coplanar and connected through an atomic scale contact. Second: we soon realized that, unlike the case of metallic nanocontacts, the conductance of "bulk" graphene is not much larger than the quantum of conductance. Therefore, a detailed study on how the conductance depends on the size of the contact, interpolating between the atomic and the macroscopic limit was in order. Finally, there are now several papers reporting experiments and theoretical calculation on transport measurements in graphene nanocontacts [1, 2, 3, 4].

1.1 Nanoelectronics

In modern society, it has become fundamental the improvement of the efficiency alongside the miniaturization in order to create new technology. In the last few decades the number of transistor that can be fitted in a chip has been doubling with each generation following the trend predicted by Moores's Law [5]. Simultaneously, computers have been increasing its computational power exponentially. In order to keep this trend, it is necessary to study in detail smaller structures.

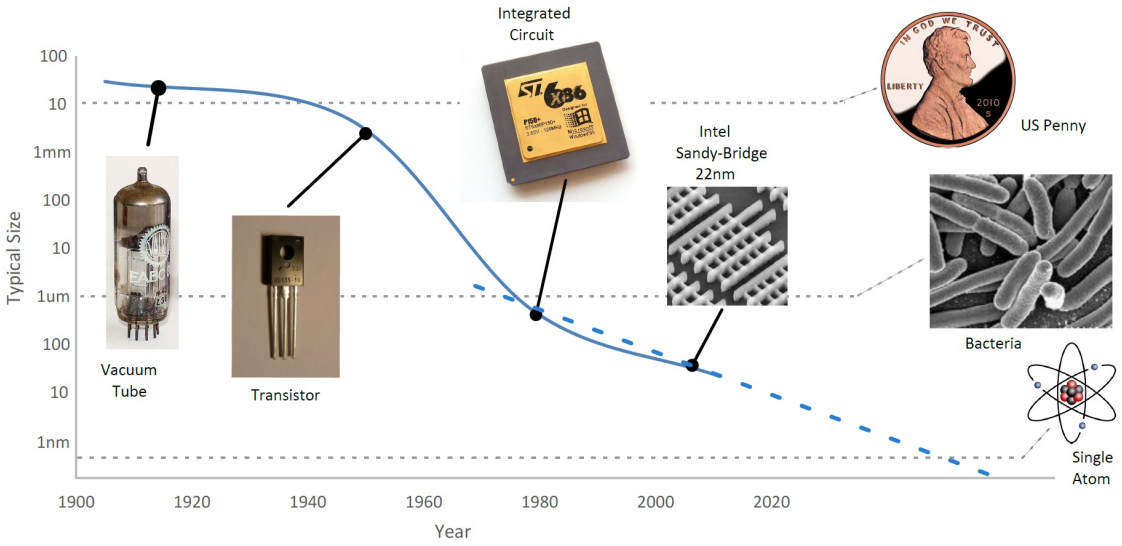

Figure 1.1: Evolution of the scale of transistor manufacturing process in time and the prediction of single atom transistor technology [6].

Figure 1.1 shows how the size of the transistor manufacturing process has been decreasing since the creation of the first transistors. To date, the goal of making small systems formed by a few atoms has been pursued. Current transistor manufacturing process size is in the 5 nm range. As a result, nanoscience has come to play a major role in electronics. Introduced by Richard P. Feynman in the talk "There's Plenty of Room at the Bottom: An invitation to enter a new field of physic" [7], in a conference at Caltech, the nanoscience tries to control and study the science of devices and materials at the nanometer scale ($10^{-9}m$). One of the greatest discoveries was to found that many of the well known characteristics of a material in bulk can change dramatically at the nanoscale. The effects of the quantum world start to became very noticeable at this scale and physics plays a fundamental role, where studying the materials at the quantum level has been an extraordinary task.

Studying nanometric systems from a theoretical point of view has become an extremely useful complementary tool to experimental research, helping to understand the measurements, saving time and expenses when working with materials that are difficult to synthesise and also predicting interesting properties in devices yet to be made. Given the well known limitations of analytical methods, most of the modelling in nanoelectronics is carried out using computational methods. As a consequence, many theoretical models had been developed to overcome this limitation letting us to get an insight into the interesting properties at the atomic scale using computational methods in a reasonable amount of time.

This topic has been widely studied for metals, going from three-dimensional materials (bulk) to single atom constrictions between the electrodes. However, in the present work we will focus on the electronic transport properties of atomic sized contacts studying similar structures with graphene, a two-dimensional semiconductor, using tight binding models

and Green's functions formalism to solve the transmission probability in the Landauer formula.

1.2 Quantum effects at the nanoscale

1.2.1 Reminder of classical theory

One of the earliest successful descriptions of the electronic transport in macroscopic metallic systems is given by Drude model [3, 8]. This model is based on the kinetic theory of gases. The electrons behave as solid spheres moving in straight line until they collide when an external electric field is applied.

The kinetic energy of the electrons is not equal to the contribution from the electric field ($q\vec{E}$). Instead, we need to consider that the collisions are taking away the energy from the electrons.

$$m\frac{d\vec{v}}{dt} = q\vec{E} + \vec{f} \tag{1.2.1}$$

This contribution, $\vec{f}$, can be modeled as a velocity depending term when we work with average velocities and so we can obtain :

$$m\frac{d\bar{v}}{dt} = q\vec{E} - m\frac{\bar{v}}{\tau} \tag{1.2.2}$$

being τ the mean free time, where the probability of an electron suffering a collision per unit of time is $1/\tau$. This equation allows us to define the average velocity of the electrons in the metal:

$$\bar{v} = \frac{qE\tau}{m} \tag{1.2.3}$$

Knowing the characteristic velocity and the mean free time, we can obtain the main free path between collisions, $l = \tau v$.

Following the gas description for the electron, we consider a box with area A and length δd in a macroscopic wire, where the current is $I = \Delta Q/\Delta t$. For an electron gas with a density n the amount of charge is given by $\delta Q = enA\delta d = enAv\delta t$ and so, the current is:

$$\frac{\delta Q}{\delta t} = enAv \tag{1.2.4}$$

Using the description for the velocity and EL=V where L is the length of the wire, the

current is described as follows:

$$I = \frac{e^2 n\tau}{m}\frac{A}{L}V \tag{1.2.5}$$

The Ohm's law tell us that the current is proportional to the electrical potential, $I = V/R$. The proportionality constant R accounts for the resistance of the system and its inverse $G = 1/R$, for the conductance. Taking this into account in the current description from Drude model, we obtain the diffuse transport description of the conductance:

$$G = \frac{e^2 n\tau}{m}\frac{A}{L} \tag{1.2.6}$$

This equation has three length scales: L, $\sqrt{A}$ and the mean free path $l = \tau v$, where v would be the typical velocity of electrons. The diffusive description implicit in the Drude model breaks down when the mean free path is larger than L or $\sqrt{A}$. Quantum effects need to be accounted when the Fermi wavelength is larger than one of these length scales. Because of this, the way we have to understand and to compute the conductance is radically different at the nanoscale. We have to take into account the complex wave function of electrons and study its quantum characteristics to define the conduction. This behaviour is defined by the electronic configuration of the atoms in contact.

1.2.2 Conductance of metallic nanocontacts

In a wide class of situations, nanoscale conductors are in series with macrosopic conductors. As a result, the resistance of the whole system is governed by the contribution of the nano-conductor, which makes it easier for its experimental determination. For the theory, the challenge is to compute the conductance at the nanoscale. Here, the so called Landauer formalism is the optimal method [9]. In this formalism, we solve a scattering problem to obtain the conductance. For that matter, we divide the system in, at least 3 parts: a nanoconstriction and a minimum of two electrodes attached to it. This will be related to the transmission probability of the electron for crossing the material. The scattering formalism can be summarized with the Landauer formula derived in further sections:

$$G = \frac{2e^2}{h}\sum_{n=1}^{N} T_n \tag{1.2.7}$$

where e is the charge of the electron, h the Plank's constant, T_n represents the transmission probability in the channel (n), where each channel are roughly related with the extended states of the electrodes. The 2 factor corresponds to spin degeneracy. We thus see that the conductance for the case of a single channel with perfect transmission $T = 1$ is given

by $G_0 = 2e^2/h$, which is known as the quantum of conductance.

Landauer formalism provides the natural framework to describe the conductance in atomic scale constrictions. There, the number of channels is roughy given by the valence of the atoms. For instance, the observation of $G = G_0$ for atomic contacts of gold relates to the fact that transmission is roughly 1 for the s electrons that dominate conductance in this system

In order to measure the quantum of conductance expected for gold we need to reproduce experimentally the formation of a single atom contact by reducing the section between the electrodes until reaching the nanocontact [10, 11, 12]. The break junction technique is the base to perform this kind of measurements. There are two main types of set-up. First, a mechanically controlled break junction (MCBJ) [13], deforming a extremely small junction between the metallic electrodes until it breaks. In the last steps, before total rupture, a single atomic contact is made. On the other hand, we can use a scanning tunnel microscope (STM) by approaching and retracting the tip and the sample in order make atomic-sized metallic contacts (STM-BJ) [14] (Figure 1.2 (b)). In both of them, the conductance is measure as a function of the displacement associated with the voltage applied in the piezoelectric device as seen in Figure 1.2(a).

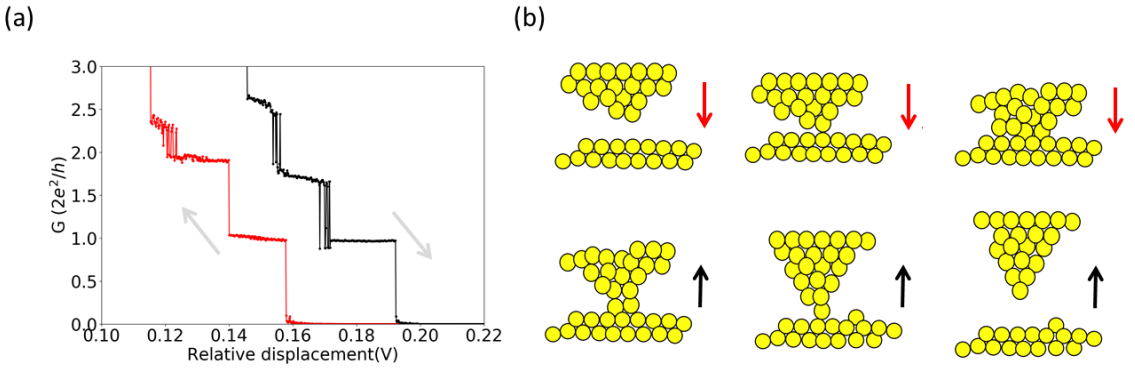

Figure 1.2: (a) Measurements of the rupture (black line) and formation (red line) of gold junction performed by a scanning tunnel microscope based break junction (STM-BJ) technique at 4.2 K from LT Nanolab, Department of Applied Physics from University of Alicante. (b) Schematic representation of the formation and rupture of the contact between the tip and the sample in a STM-BJ experiment [15].

As seen in Figure 1.2 (b), the top images correspond to the formation of the contact in the STM-BJ technique. As the tip approaches the sample, the first contact is made with a single gold atom and the conductance goes from the tunnel regime to the contact regime. In Figure 1.2 (a) we can see this in the red line with the first step as the contact is made, achieving a quantum of conductance. From there, as more atoms from the tip are in contact with the sample, the conductance increase in a quantized manner (integers of G_0). The top images from panel (b) represents the rupture of the contact. In the last step, before breaking the junction, a single atomic contact is achieved. In panel (a) this can be seen in the black line, for the last contact (a single atom), the plateau corresponds to 1

G_0. There is an extended bibliography of experimental data and theoretical calculations of the conductance in metallic nanocontacts [15]. Being a well known fact that even with a single atomic contact with a perfect channel, the device is able to achieve a conduction of at least G_0.

1.3 Electronic properties of graphene

In 2010, Andrei Geim, Konstantin Novoselov and co-workers [16] received the Nobel prize by the isolation of a single carbon layer graphite by mechanical exfoliation. Their result contradicts what L.D. Landau y R.E. Peierls predicted, i.e. the impossibility of isolate 2D monoatomic crystal layers due to the lack of thermodynamic stability [17, 18]. Each layer is a two dimensional structure known as graphene, term coined by Hanns-Peter Boehm while studying extremely thin flakes of graphite [19].

The strong binding among the carbon atoms and the honeycomb lattice makes graphene a material with extraordinary characteristics such as high strength [20] and excellent electronic and thermal conduction [21]. Since its experimental appearance, the rise of graphene [22] has attracted the scientists attention to 2D structures, used as a base for different studies focus on 2D materials.

The two quantities that appear in all formulas describing insulators and conductors, namely, the band-gap and the density of states at the Fermi energy, are zero in graphene. As a result, graphene has quite peculiar electronic properties. Graphene is zero gap semiconductor. The point where the conduction and the valence bands meets are called the Dirac points.

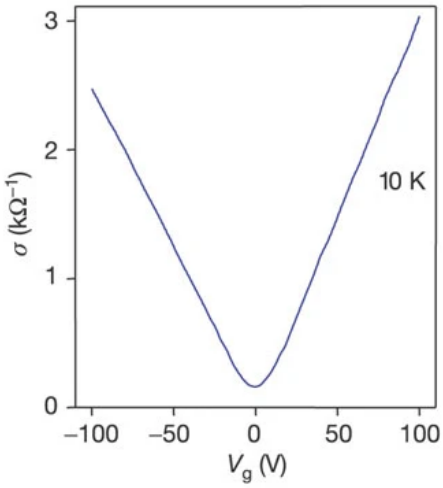

Figure 1.3: Experimental conduction of graphene as a function of the gate voltage applied [23].

Another important aspect about charge transport in graphene is its ambipolar behavior. This implies that charge carriers can be tuned continuously between holes and

electrons by supplying the necessary voltage [24]. Under negative gate bias, the Fermi level drops below the Dirac point, introducing a significant population of holes into the valence band. Under positive gate bias, the Fermi level rises above the Dirac point, promoting a significant population of electrons into the conduction band.

In semiconductors, transport is dominated by carriers at the extreme of the bands with parabolic dispersion. As a result, their description can be done using a Schrodinger equation with an effective mass. In graphene, bands are linear. Those are at the junction of the Dirac cones (Figure 1.3), this conic geometry defines the unique nature of its charge carriers. The relevant effective model for these bands is the Dirac equation [25]:

$$E_F = \hbar v_F k_F \tag{1.3.1}$$

where the speed is set at $v_F \sim 10^6 m/s$ or $c/300$, being c the speed of light in vacuum.

In contrast to the conductance in conventional two-dimensional materials, graphene shows conductance at the Dirac point that is geometry dependent. The electronic transport is related to evanescent modes [26]. A distinct feature of a 2D massless Dirac fermion system is that the minimum of conductance is predicted to be an universal value of $G_0 = 4e^2/\pi h$ for both ballistic and disordered cases [22]. Another studies, [23, 27] found an universal, but larger, value of $G_0 = 2e^2/h$. This π factor was complicated to explain, thus generating a debate between theory and experimental data [28, 29, 30, 31, 32].

By narrowing the size of the graphene sheet in one of the two direction, we can reduce the dimensionality of the system. These stripes of graphene that have a finite width and an infinite length (from the electronic point of view) are called graphene nanoribbons (GNRs). In these types of structures, the minimum of conductance is often reported experimentally to be a quantum conductance, $G_0 = 2e^2/h$ [28]. However, it is also possible to recover the original theoretical value with the π factor by reducing the length in very wide ribbons, achieving ballistic transport [33].

The experimental results can be explain with the Klein paradox [34]. It states that the quasiparticles in graphene, that have a perfect electron-to-hole conversion at a potential barrier, will have a probability of one of tunneling through the barrier [35]. This guarantees the absence of localization [32, 36] and the existence of a finite minimum conductance measured in several works experimentally [37, 16] and theoretically [38, 39]. This makes graphene ribbons suitable to be used in all sort of electronic devices.

1.4 Motivation

Initially, the main focus of this work was to study the electronic transport between two non-coplanar graphene nanoribbons. We wanted to study the conductance as a function of the angle. The idea behind this came from an article about dynamic tunneling junctions at the atomic intersection of two twisted graphene edges [40]. In this experiment, in order

to study the electronic transport through a graphene atomic-sized contacts, two graphene flakes were approached in a certain angle as seen in Figure 1.4 (a).

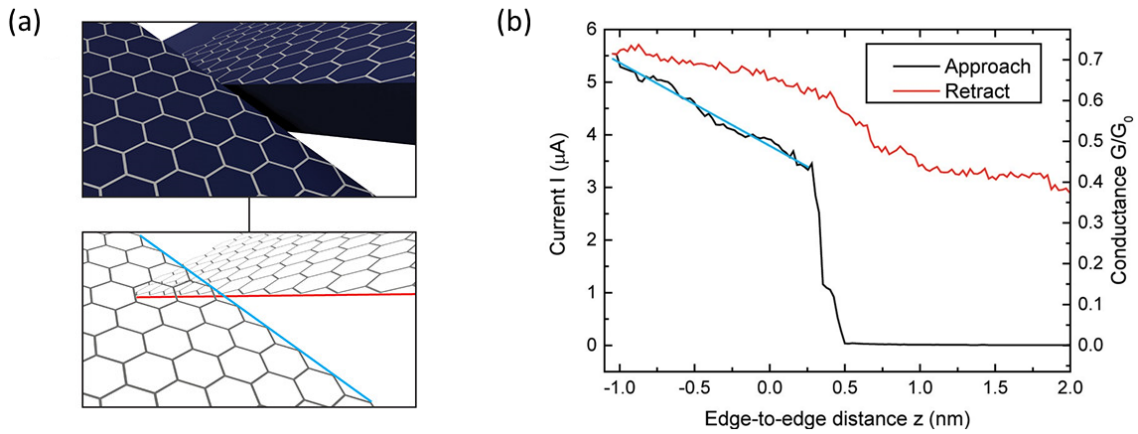

Figure 1.4: (a) Schematic representation of the contact between two graphene nanoribbons in a certain angle. (b) Conductance as a function of the distance between the GNRs in the formation and the rupture of the junction. Images from [40].

The conductance was measured as they approached and retracted the ribbons. From the results presented in Figure 1.4 (b), while approaching, they found a conductance of approximate $0.4\,G_0$ for the first contact. Taking into account the contribution of the electrodes used, the real value they estimated is around 0.8 and $1.3\,G_0$. While stretching, they observed that a similar value is maintained along a few manometers. This result suggest the formation of a carbon atomic chain before the junction is broken.

As we started to delve in this question, we realized that the conductance in graphene nanocontacts, needed in order to model the electronic transport between non-coplanar ribbons, are far from the metallic nanocontacts. Therefore, we decided to perform a detailed study on the conductance of different types of contacts as a function of the geometry of the contact, the constriction and electrodes widths and the Fermi energy.

This topic is of interest since in recent years some works have emerged studying graphene nanocontacs, from a theoretical and experimental point of view. Going from quantum interference in graphene break junctions [1], quantized edge modes in atomic-scale point contacts in graphene [4] to mechanically tunable quantum dot in a graphene break junction [2].

Chapter 2

Methodology

The quantum properties of a system in solid state are determined by solving the Schrodinger equation for the electrons. We have to take in consideration the kinetic and the potential energy of any particle in the system. With N particles, the number of variables needed in order to describe only the position are $3N$. With the current mathematical tools we can not solve more than a two body problem, hence, we need to make approximations in order to solve the problem for bigger systems.

From the different models and approximations developed, the majority of the *ab-initio* calculations of the electronic structure are based on density functional theory (DFT). This approach is able to reduce the number of variables and get very accurate results. However, the computational cost is high for systems with hundreds of atoms. Therefore we may need a more efficient however less accurate model. In this work we use the tight binding model that offers a good relation between accuracy and computational power in materials as graphene.

2.1 Tight binding model

In ordinary systems, in order to describe the behaviour of one electron, many variables are needed. The interaction of the electron and the other electrons in the system, also the interaction with the the nuclei of the atoms. For crystalline systems, we can make an approximation by assuming that the Hamiltonian of the complete structure can be described by the Hamiltonian of a single atom due to the repetition in the lattice. This model is already well described in many textbooks [8, 9]. We are going to introduce briefly the model, we can start by defining the Hamiltonian of a single atom as follows:

$$H = H_{at} + \Delta U \tag{2.1.1}$$

where H_{at} is the Hamiltonian describing the single atom and ΔU is all the potential acting

on that atom produced by the rest of the system. We can assume that the interaction fades away with the distance from the centre of the atom. Therefore, $\Delta U \longrightarrow 0$ and we can define the energy of the particle with the Schrödinger's equation as follows:

$$H\Psi_{nk}(r) = E_{nk}\Psi_{nk}(r) \tag{2.1.2}$$

where n is the index of the band and k is the wavevector in the first Brillouin zone.

For the energy of the atom itself, we can apply the H_{at} with the atomic wavefunctions Φ_i in the Schrödinger equation, and so we obtain:

$$H_{at}\Phi_i(r) = \epsilon_i\Phi_i(r) \tag{2.1.3}$$

The overlap integral takes into account the relation between the wave functions of two different positions in the lattice ($r = 0$ and $R \neq 0$) and can be defined as:

$$\gamma(|R|) = \int \Phi_i^*(r)H\Phi_i(r+R)dr \tag{2.1.4}$$

As established before, the overlap of the function from other position in the crystal should decay rapidly from the center of the atom under study. Therefore, we can make the approximation for the atomic orbitals as orthonormal functions, being the overlap integral zero, in any position of the system but centred on the atom itself.

$$\int \Phi_i^*(r)\Phi_j(r+R)dr = 1 \cdot \delta_{i,j}(R=0) \tag{2.1.5}$$

To apply this approximation, we have to make sure that the states for the single atom follows the Bloch's theorem [8], the single atomic orbital does not apply to the theorem, in order to achieve this we have to make a linear combination of atomic orbitals (LCAO). We are going to particularize for the case of a single band. By making this change we will comply with the criteria of Bloch functions thanks to the $1/\sqrt{N}$:

$$\Psi_{nk}(r) = \frac{1}{\sqrt{N}}\sum_R e^{ik\cdot R}\Phi_n(r-R) \tag{2.1.6}$$

where N are the possible sites in the crystal and R the translation vector in the real space.

In order to define the relation between the energy and the wavevector, we need to calculate the value of the energy defining the dispersion relation as follows:

$$E(k) = \int \Psi_k^*(r)H_k(r)dr \tag{2.1.7}$$

Now, if we apply the linear combination of atomic orbitals, we end up with the next expression:

$$\begin{aligned} E(k) =& \frac{1}{N} \sum_{R} \sum_{R'} e^{ik\cdot(R'-R)} \int \Phi_s^*(r-R) H \Phi_s(r-R') dr \\ =& \frac{1}{N} \sum_{R} \sum_{R'} e^{ik\cdot(R'-R)} \int \Phi_s^*(x) H \Phi_s(x-(R'-R)) dx \end{aligned} \tag{2.1.8}$$

In the last step we change the spatial variable r to $x = r - R'$, and so, the Hamiltonian remains the same due to the periodicity in the system. Then, as we are summing over all the translation vectors, we can change R and define a translation vector as $R' - R = R''$, also, a position in the lattice. Making the change in the equation, we obtain:

$$E(k) = \frac{1}{N} \sum_{R} \sum_{R''} e^{ik\cdot R''} \int \Phi_s^*(x) H \Phi_s(x-R'') dx \tag{2.1.9}$$

all the terms in the sum of the translation vector are the same, this leave us with one term for every possible site in the lattice:

$$E(k) = \sum_{R''} e^{ik\cdot R''} \int \Phi_s^*(x) H \Phi_s(x-R'') dx \tag{2.1.10}$$

The next step is to split the components of the sum. As mention before, the orbitals are highly centred in each atom and decrease with the distance from the centre of the atomic site. The first term is can be obtained by making $R'' = 0$.

$$\int \Phi_s^*(x) H \Phi_s(x) dx = \int \Phi_s^*(x) \epsilon_s \Phi_s(x) dx = \epsilon_s \tag{2.1.11}$$

from the result, we obtain the energy of the orbital in a single atom.

In the other limit, for R'' being a position that is far from the atom, the energy should be zero. But if we take into account the contribution from the nearest neighbours, making the distance $R'' = \tau$, being τ the distance of the neighbour atom, we can define the dispersion relation as:

$$E(k) = \epsilon_s + \sum_{\tau} e^{ik\cdot\tau} \int \Phi_s^*(x) H \Phi_s(x-\tau) dx \tag{2.1.12}$$

The integral part of the equation is the same as the overlap integral defined before. In this model, being a semi-emphirical method, we can set the the overlap integral to a certain

neighbours as a constant that match the experimental data, called the hopping term:

$$\gamma(|\tau|) = \int \Psi_s(x) H \Phi_s(x-\tau) dx. \tag{2.1.13}$$

Finally, we obtain the dispersion relation for the single band tight binding approximation with the nearest neighbour atoms contribution:

$$E(k) = \epsilon_s + \sum_{\tau} e^{ik\cdot\tau} \gamma(|\tau|) \tag{2.1.14}$$

2.1.1 Band structure for infinite graphene

Graphene is a 2D crystal. Therefore, the reciprocal space is also 2D:

$$a_1 = a(\frac{1}{2}, \frac{\sqrt{3}}{2}) \quad a_2 = a(\frac{-1}{2}, \frac{\sqrt{3}}{2}), \tag{2.1.15}$$

with $a = \sqrt{3}a_0$ being the lattice constant and $a_0 = 1.42$Å is the distance between carbons.

In Figure 2.1, with a integer number multiplying the lattice vectors, we can recreate the crystal structure.

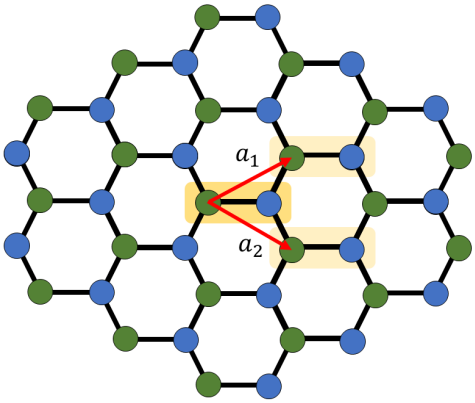

Figure 2.1: Schematic representation of the graphene unit cell and its lattice vectors in the honeycomb structure.

Each carbon atom has four electrons, three of them form the graphene structure in the plane as σ bonds. The other electron is oriented perpendicular to the plane, in a $2p_z$ orbital. The unit cell is formed by two atoms. The Hamiltonian of each unit cell will be:

$$H_{RR}(k) = H_{R'R'}(k) = \epsilon_0 \tag{2.1.16}$$

with ϵ_0 the onsite energy of each unit cell.

We can set the overlap integral as a constant t, the hopping value. Now we can define the interaction between the nearest neighbours:

$$H_{RR'}(k) = -t(e^{-ika_1} + e^{-ika_2} + 1) \tag{2.1.17}$$

The Hamiltonian for the crystal structure can be defined as follows:

$$H = \begin{pmatrix} \epsilon_0 & t(e^{i\vec{k}\vec{a}_1} + e^{i\vec{k}\vec{a}_2} + 1) \\ t(e^{-i\vec{k}\vec{a}_1} + e^{-i\vec{k}\vec{a}_2} + 1) & \epsilon_0 \end{pmatrix} \tag{2.1.18}$$

Finally, we obtain the dispersion relation for 2D graphene:

$$E(\vec{k}) = \epsilon_0 \pm |t|\sqrt{4cos_2(k_y\frac{a}{2}) + 4cos(k_x\frac{\sqrt{3}a}{2})cos(k_y\frac{a}{2}) + 1} \tag{2.1.19}$$

Now if we plot the dispersion relation as function of the wave vector for each possible dimension, we obtain the 2D band structure of graphene.

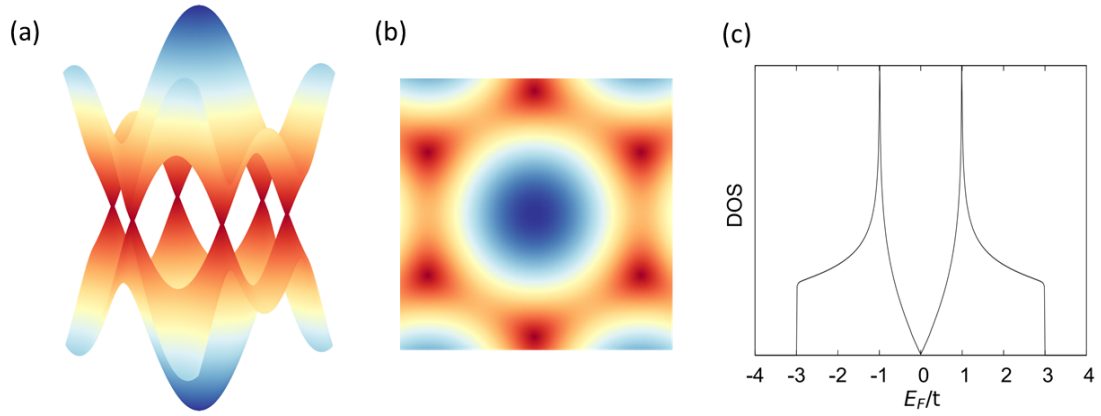

Figure 2.2: (a) Representation of the 2D band structure with the energy as a function of k_x and k_y. (b) Projection in the plane of the graphene band structure. The red points represent the Dirac points. (c) Density of states (DOS) of 2D graphene. Image modified from [41].

As described in the introduction chapter, graphene has Dirac cones on its bands, responsible for many of its electronic properties. In the Figure 2.2 (b), we can see the Dirac points as red spots, the junction between the Dirac cones, as we can see in (a). So, with the tight binding model we can reproduce the well known characteristics of graphene band structure. From (c) we can see that there is no density of states at the Dirac point. In the semi-classical formulation of the Drude model we use the density of states at $E_F = 0$

instead of the charge density n and the electron mass m. With this approach, Drude model would predict $G = 0$ at the Dirac point, contrary to the experimental values discussed in section 1.3.

2.1.2 Band structure of graphene nanoribbons

We can cut thin stripes on infinite two-dimensional graphene in different directions. These allows us to obtain graphene ribbons with different type of edges. If we make the ribbons thin enough it can be considered a one dimensional system. The most known edges of graphene ribbons are zigzag and armchair, as seen in Figure 2.3 (a) and (b) respectively. The width is defined with the number of dimers in the finite direction.

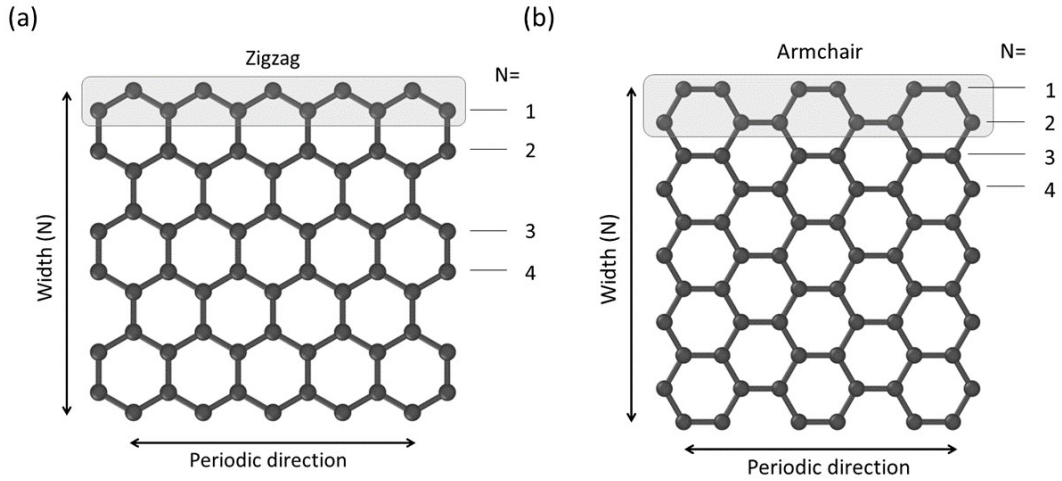

Figure 2.3: Representation of two types of nanoribbons edges: (a) zigzag and (b) armchair, with the corresponding notation for the widths for each case.

We are going to apply the tight binding model to those ribbons (armchair and zigzag). The bands are obtained by numerical diagonalization of the Bloch matrix and we have coded a python program for such task.

2.1.2.1 Armchair

The band structure of armchair graphene ribbons in Figure 2.4 shows the values of the Fermi energy E_F scaled with the overlap integral value (the hopping term) t as a function of the wave vector k. In this edge type, the widths of the ribbons is what determines the behavior of the system. We can follow the rule $N = 3M - 1$, where M is an integer number, to determine if an armchair ribbons has a gap or if the valence and conduction bands meet at zero energy as shown in Figure 2.4 [42]. The end result is similar to the projection of the infinite graphene crystal in the armchair direction.

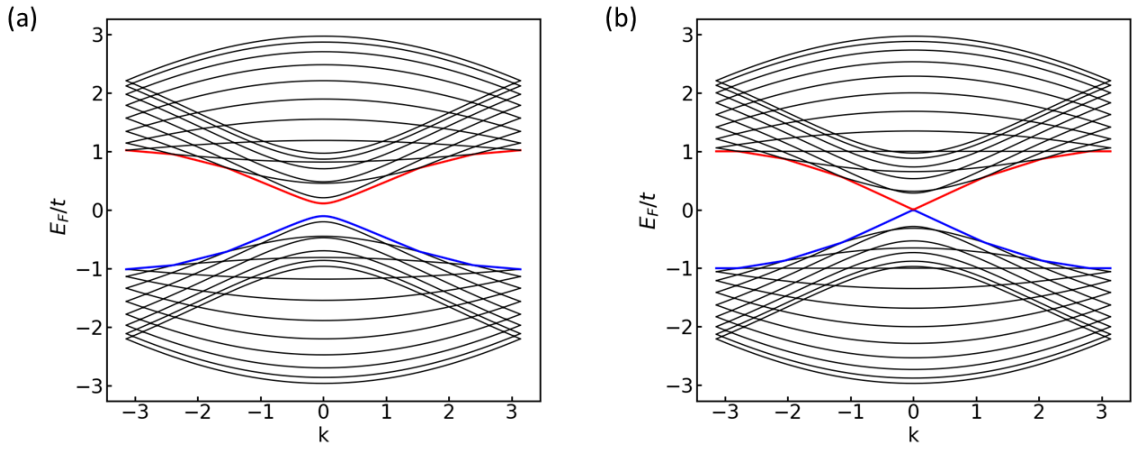

Figure 2.4: One dimensional band structures of an armchair graphene nanoribbon with (a) N = 16 (b) N = 17, showing an insulator and a metallic behaviour respectively. Marked in red and blue the conduction and the valence band.

By plotting the density of states (DOS) of armchair nanoribbons we can see that for widths that follows the rule mention before, there are states at zero energy (Figure 2.5 AC-17) and not for the others (Figure 2.5 AC-16). We can also see that the gap reduces inversely proportional to the width (Figure 2.5 AC-71. The DOS of the wider ribbon becomes quite similar to the one of 2D graphene, shown in Figure 2.2 (c).

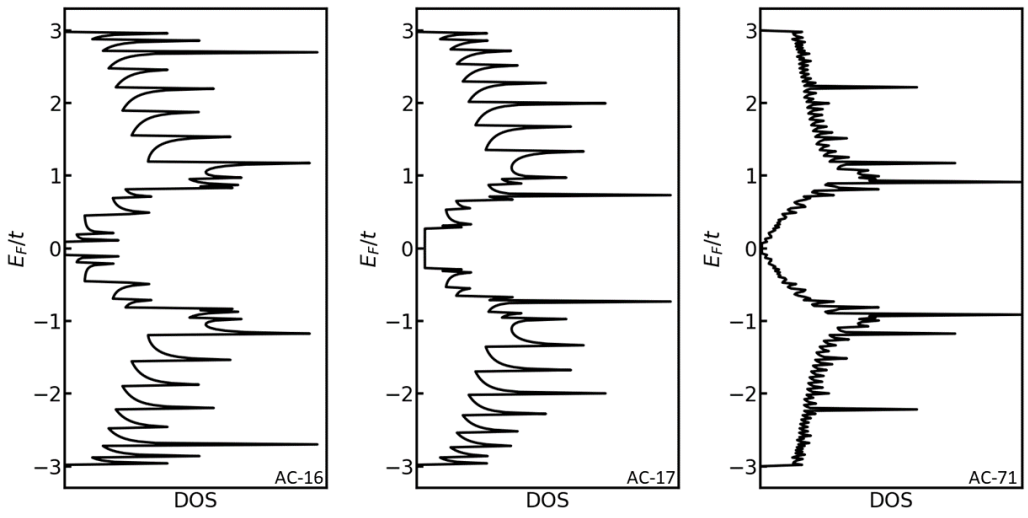

Figure 2.5: Density of states in armchair nanoribbons with N=16, 17, 71.

2.1.2.2 Zigzag

In the case of zigzag edge a new feature arise from making graphene ribbons. In contrast to the projection that can be made from infinite graphene bands on the zigzag

direction, the structure of the bands has some differences. As we can see in Figure 2.6, two flat bands appears at zero energy where valence and conduction bands meet. The origin of these bands is not the intrinsic band structure of graphene, it is from the edge states. The wave function resides completely on the edges of the ribbon and the bands gets flatter as we make the ribbon wider [42].

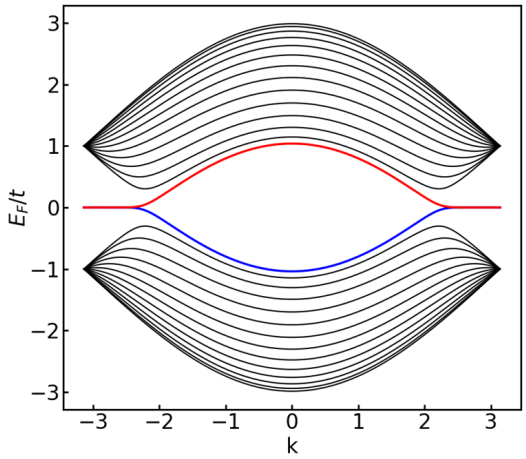

Figure 2.6: Band structure of a zigzag graphene nanoribbon with N = 14, blue and red lines are valence and conduction bands respectively.

Therefore, the electronic transport in zigzag edges is completely determined by the edge states [43] and the flat bands at zero energy (Figure 2.7). This type of systems shows a metallic behavior for any ribbon width.

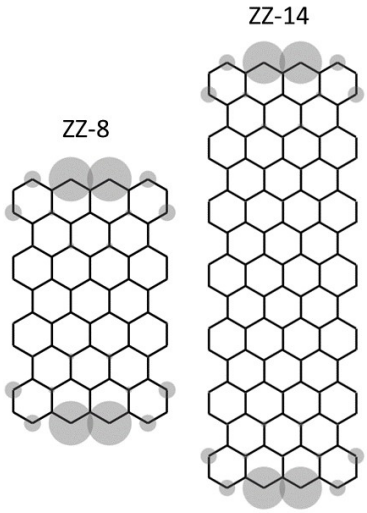

Figure 2.7: Edge states of zigzag nanoribbons. Representation of the wave function in zigzag ribbons with N= 8, 14 as grey circles for the flat bands.

With the edges states coming from the flat bands at zero energy, the density of states (DOS) is expected to show sharp peaks at the Dirac point.

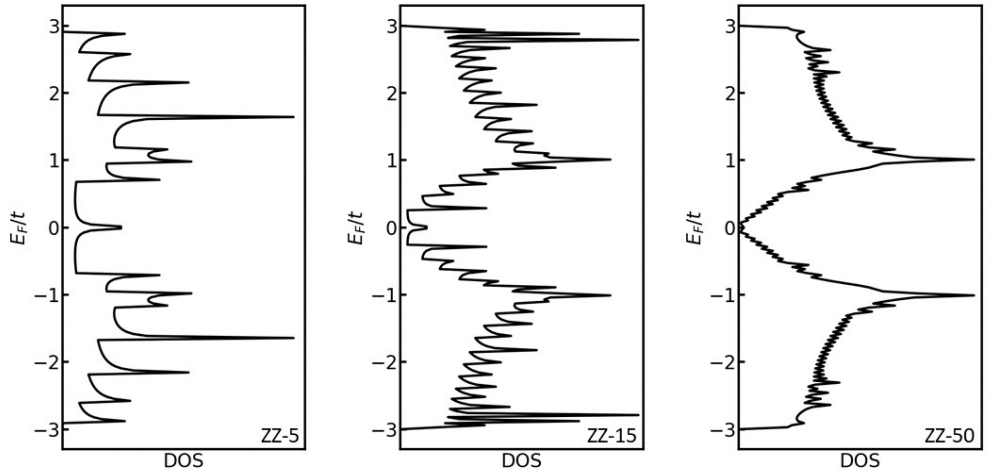

Figure 2.8: Density of states in zigzag nanoribbons with N=5, 15, 50.

In Figure 2.8, we can see the expected peaks at zero energy. For smaller widths the contribution of those is greater. Although, as we make the ribbon wider the contributions starts to be negligible. Another characteristic that we can extract from the graph is how, as the width of the ribbon increases, the relative weight of the $E_F = 0$ edge states is reduced and the DOS of 2D graphene (2.2 (c)) starts to emerge.

2.1.3 Dependence of the third nearest neighbour

One step further in the tight binding model approximation is to add the terms corresponding to the hopping between not only the nearest neighbours but also the next nearest or even third neighbours. In the case of graphene, next nearest neighbours provokes a rupture of the electron-hole symmetry but the effects in the electronic properties can be neglected [44]. Therefore, we can improve the model by taking into account only the third nearest neighbours, giving similar results to the ones with ab initio calculations [45]. We can define the third nearest neighbour hopping term as $t_3 = 0.15\,t$ and is presented on the system as seen in the visual representation of Figure 2.9.

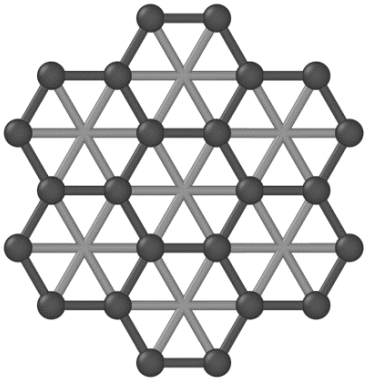

Figure 2.9: Graphene lattice with a visual representation of third nearest neighbour hopping in light gray.

Although the system properties are expected to not change drastically, some difference can appears. Now we present the bands for the exact same systems as in the nearest neighbour calculation:

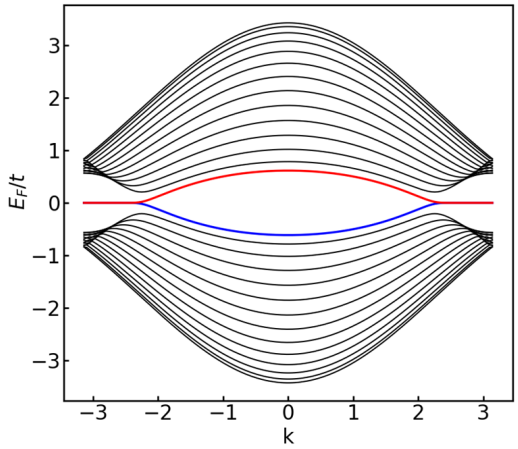

Figure 2.10: One dimensional band structure of a zigzag graphene nanoribbon with N = 14 considering third nearest neighbours hopping contribution.

From the zigzag band structure (2.10), the gap is still zero at $E_F = 0$. On the other hand, the shape has changed. We found the bands closer to the Dirac point. This is in accordance with the increase on the number of channels that we just add to the system.

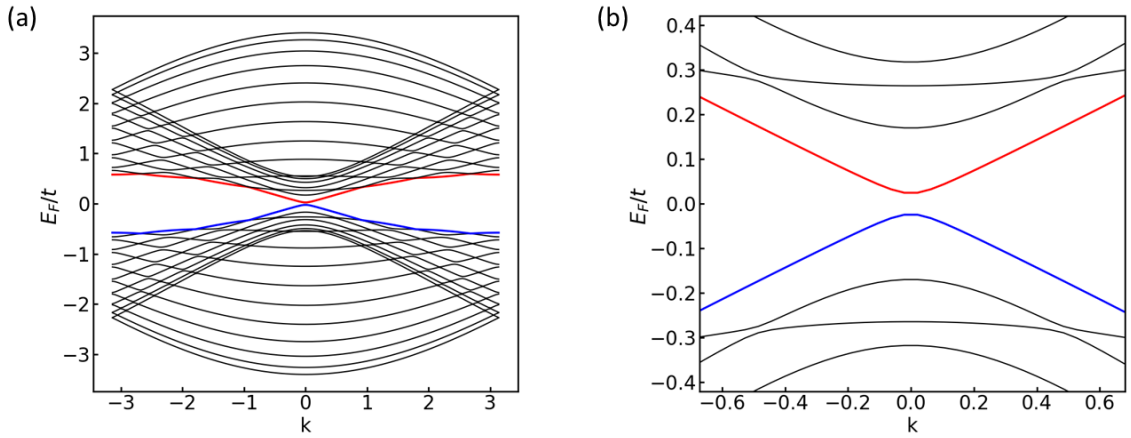

Figure 2.11: (a) One dimensional band structure of an armchair graphene nanoribbon with N = 17 considering third nearest neighbours hopping contribution. (b) Zoom in the Dirac point highlighting the gap.

In the case of armchair ribbons, we can see from 2.11 that a small gap appears when taking into account third nearest neighbour contribution. Therefore, this could affects the electronic transport calculations.

2.2 Landauer formula

The Landauer approach [46, 47, 48] is the most used theoretical formalism to study the coherent transport in materials with a nanometric size. The main idea of this approach is to ignore inelastic interactions, a transport problem can always be viewed as a scattering problem. The transmission probability for charge carriers to cross from one electrode to the other through a contact is related to the transport properties of the material and therefore its electrical conductance.

The derivation can be found in [49]. In this case, we start by defining the current for a system with multiple terminals:

$$I_p = \int i_p(E)dE \tag{2.2.1}$$

where i_p is given by the total transmission from terminal q to terminal p (T_{pq}) for a certain energy E:

$$i_p(E) = \frac{2e}{h} \sum_q \left[T_{qp}(E)f_p(E) - T_{pq}(E)f_q(E)\right] \tag{2.2.2}$$

being $f_{p,q}$ the Fermi function for the correspondent terminal:

$$f_p(E) = \left[exp\left(\frac{E - \mu_p}{k_B T} \right) + 1 \right]^{-1} \tag{2.2.3}$$

Assuming that at the equilibrium there is no current, the transmission must satisfy:

$$\sum_q T_{qp}(E) = \sum_q T_{pq}(E). \tag{2.2.4}$$

considering that assumption and taking into account that there is no inelastic scattering inside the device, we can approximate the current in the following manner:

$$i_p(E) = \frac{2e}{h} \sum_q T_{pq}(E) \big[f_p(E) - f_q(E) \big]. \tag{2.2.5}$$

The system must comply with having a net current of zero:

$$I_p = \int i_p(E) dE = 0 \tag{2.2.6}$$

If the bias $(\mu_1 - \mu_2)$ is small compared to the , $k_B T$ energy, we can linearize the system:

$$I_p = \sum_q G_{pq} \big[V_p - V_q \big], \text{ where } V_p = \frac{\mu_p}{e} \tag{2.2.7}$$

where the conductance is given by:

$$G_{pq} = \frac{2e^2}{h} \int T_{pq}(E) \left(- \frac{\partial f_0}{\partial E} \right) dE \tag{2.2.8}$$

If we work at low temperature, we can approximate the conduction only by its transmission probability:

$$G_{pq} = \frac{2e^2}{h} T_{pq}(E_f) \tag{2.2.9}$$

The results shows that a perfect single channel in a material between two electrodes has a finite resistance, given by the universal quantity of $G_0 = 2e^2/h$. Being the conductance proportional to the transmission probability with a constant of proportionality that is the quantum of conductance.

2.3 Calculation of the transmission matrix

Following the scattering formalism, we can introduce Green's functions technique in order to use the tight binding Hamiltonians to calculate the transmission probability and therefore the conductance.

We work with a two lead device example. We will propagate the states that are inside the lead into the device region using a Green's function technique. We call these states the scattering states, and from them, the total current that goes between the leads can be calculated. We can define the Hamiltonian for a single particle as a matrix operator as follows:

$$H = H_0 + V = \begin{pmatrix} H_L & 0 & 0 \\ 0 & H_d & 0 \\ 0 & 0 & H_R \end{pmatrix} + \begin{pmatrix} 0 & V_{Ld} & 0 \\ V_{dL} & 0 & V_{dR} \\ 0 & V_{Rd} & 0 \end{pmatrix} \tag{2.3.1}$$

where the $H_{L,R}$ and H_d are the Hamiltonians describing the leads isolated from the system and the device region; V is the interaction between the electrodes and the device. Therefore we achieve a Hamiltonian that fully describe the particle in the three regions taking into account the interactions between them.

We can define three operators in order to indicate the region in which we are working, one for each of the regions. The device region P_d and the left and right leads $P_{L,R}$. The sum of all three must be unitary ($P_L + P_d + P_R = I$) and the two leads can not be directly connected:

$$P_L = \begin{pmatrix} 1 & 0 & 0 \\ 0 & 0 & 0 \\ 0 & 0 & 0 \end{pmatrix} \quad P_d = \begin{pmatrix} 0 & 0 & 0 \\ 0 & 1 & 0 \\ 0 & 0 & 0 \end{pmatrix} \quad P_R = \begin{pmatrix} 0 & 0 & 0 \\ 0 & 0 & 0 \\ 0 & 0 & 1 \end{pmatrix} \tag{2.3.2}$$

The Green's function can be defined as the inverse of the energy minus the Hamiltonian of the system. There are two functions in relation to the direction of the particle, the retarded and the advanced. We only need the retarded Green function and we can define it using the eigenstates of the Hamiltonian:

$$G(E) = [E + i\delta - H]^{-1} = \int dE' \sum_m \frac{|\Psi_m(E')\rangle \langle \Psi_m(E')|}{E + i\delta - E'} \tag{2.3.3}$$

where m indexes any degenerate states at a given energy and the infinitesimal energy $\delta = 0+$ is used to select the retarded response in the system.

2.3.1 Partition method

Following the matrix notation we can write the Green's function operator:

$$G = \begin{pmatrix} G_L & G_{Ld} & G_{LR} \\ G_{dL} & G_d & G_{dR} \\ G_{RL} & G_{Rd} & G_R \end{pmatrix} \tag{2.3.4}$$

We can compute the device part in Green's function terms using the relation between the function itself and the Hamiltonian, $(E - H)G(E) = 1$:

$$\begin{pmatrix} E - H_L & -V_{Ld} & 0 \\ -V_{dL} & E - H_d & -V_{dR} \\ 0 & -V_{Rd} & E - H_R \end{pmatrix} \begin{pmatrix} G_L & G_{Ld} & G_{LR} \\ G_{dL} & G_d & G_{dR} \\ G_{RL} & G_{Rd} & G_R \end{pmatrix} = \begin{pmatrix} 1 & 0 & 0 \\ 0 & 1 & 0 \\ 0 & 0 & 1 \end{pmatrix} \tag{2.3.5}$$

Three expressions can be obtained from the second column in the matrix operator:

$$\begin{aligned} (E - H_L)G_{Ld} - V_{Ld}G_d &= 0 \\ -V_{dL}G_{Ld} - H_dG_d - V_{dR}G_{Rd} &= 1 \\ -V_{Rd}G_d + (E - H_R)G_{Rd} &= 0 \end{aligned} \tag{2.3.6}$$

we are interested in using the first and the last one, so we obtain the next expressions:

$$\begin{aligned} G_{Ld} &= g_L V_{Ld} G_d \\ G_{Rd} &= g_R V_{Rd} G_d \end{aligned} \tag{2.3.7}$$

where $g_{L,R} = [E - H_{L,R}]^{-1}$ corresponding to the leads functions. Applying these equations to the result from 2.3.6 we can define:

$$G_d = [E - H_d - \Sigma_L - \Sigma_R]^{-1} \tag{2.3.8}$$

obtaining the Green function of the device as a function of the leads self-energies:

$$\begin{aligned} \Sigma_L &= V_{dL} g_L V_{Ld} \\ \Sigma_R &= V_{dR} g_R V_{Rd} \end{aligned} \tag{2.3.9}$$

The spectral function of the Green's Function can be defined as:

$$A(E) = i\big(G(E) - G^{\dagger}(E)\big) = 2\pi \sum_{n} |\Psi_n(E)\rangle \langle \Psi_n(E)| \tag{2.3.10}$$

Finally, we define the coupling matrices using the self energies:

$$\begin{aligned} \Gamma_L &= i(\Sigma_L - \Sigma_L^{\dagger}) \\ \Gamma_R &= i(\Sigma_R - \Sigma_R^{\dagger}) \end{aligned} \tag{2.3.11}$$

2.3.2 Relation between current and transmission

With all the elements necessary defined, we can write down the current operator. In this case, we use the operator P_R to describe the electrons in the right lead. If we make the time derivative of the right lead operator we get:

$$J_R = 2e\dot{P}_R = \frac{i2e}{\hbar}[H, P_R] \tag{2.3.12}$$

being the factor two a representation of the spin degeneracy.

The current between the leads can be calculated using the states corresponding to the left lead onto the current operator of the right lead:

$$\begin{aligned} j^{(L)} &= \langle \Psi^{(L)}| J_R |\Psi^{(L)}\rangle \\ &= \frac{i2e}{\hbar}\Big(\langle \Psi_d^{(L)}| V_{dR} |\Psi_R^{(L)}\rangle - \langle \Psi_R^{(L)}| V_{Rd} |\Psi_d^{(L)}\rangle \Big) \\ &= \frac{i2e}{\hbar}\Big(\langle \Psi_d^{(L)}| V_{dR} g_R V_{Rd} |\Psi_R^{(L)}\rangle - \langle \Psi_R^{(L)}| V_{dR} g_R^{\dagger} V_{Rd} |\Psi_d^{(L)}\rangle \Big) \\ &= \frac{2e}{\hbar} \langle \Psi_d^{(L)}| \Gamma_R |\Psi_d^{(L)}\rangle \end{aligned} \tag{2.3.13}$$

The sum of all the scattering states originated in the left lead correspond to the total current. Each scatter state $|\Psi_{d,l}^{(L)}\rangle$, with the index l:

$$\begin{aligned} j_{tot}^{L} &= \frac{2e}{\hbar} \sum_{l} \langle \Psi_{d,l}^{(L)}| \Gamma_R |\Psi_{d,l}^{(L)}\rangle \\ &= \frac{2e}{2\pi\hbar} \sum_{m} \langle m| \Gamma_R \Big(\sum_{l} |\Psi_{d,l}^{(L)}\rangle \langle \Psi_{d,l}^{(L)}| \Big) |m\rangle \\ &= \frac{2e}{h} tr\Big[\Gamma_R G_d \Gamma_L G_d^{\dagger} \Big] \end{aligned} \tag{2.3.14}$$

And so, we obtain the analogous version of the Landauer formula, in which the transmission is defined as:

$$T = tr[\Gamma_R G_d \Gamma_L G_d^\dagger] \tag{2.3.15}$$

2.4 Calculating the transmission matrix using Kwant

The calculation of the transmission matrix can has a high computational cost. In order to approach the solution in a more efficient manner we can use the recursive Green's function algorithm [50, 51, 52]. Instead of computing the full Green's function we can obtain only the useful information to compute the conductance. We also know that the tight-binding Hamiltonian is a sparse matrix, where most of the values are zero. This method is based on physical considerations and suits very well semi-infinite systems that are much longer in the direction of the leads.

The idea of recursive Green's function algorithm is to go from the Green's function of a part of the system that we know how to solve as if this part was disconnected from the rest. We take the next part that is connected to the known one and we compute the Green's function for this, emulating that is disconnected. Then we connect the two parts and couple them, thinking in the coupling as a perturbation using the Dyson equation.

The Dyson equation and the derivation can be found in [49]. This allows us to compute the transmission through the system by defining a self-consistent formula:

$$\Sigma_{1,r} = V \frac{1}{E - H_0 - \Sigma_{1,r}} V^\dagger \tag{2.4.1}$$

In order to solve the recursive Green's function, there are many software options available. For this work we are going to use the Kwant [53] software package. Kwant is a python library based on the tight binding models and highly oriented to quantum transport analysis. This software offers a simple and fast tool to obtain results with highly efficient algorithms for tasks as solving the self-consistent equations.

2.4.1 Examples with monoatomic chains

In this section we are going to present two studies using Kwant, with a simple example using monoatomic chains. First, a study on how the transmission probability changes as a function of the hopping value of the contact between two chains.

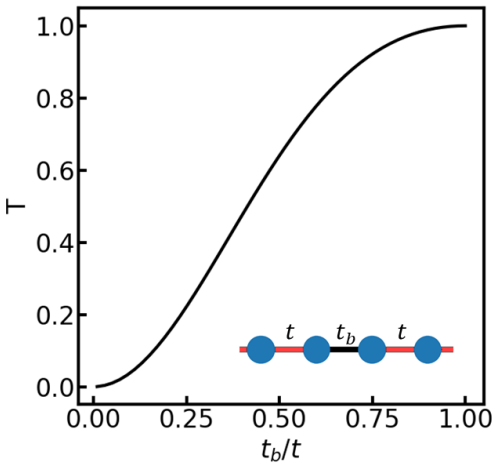

Figure 2.12: (a) Transmission probability (T) for chains with a barrier as a function of the energy for different barrier values (t_b) and a schematic representation of the the barrier (black hopping) between the monoatomic chains.

From Figure 2.12, we can see that the scaling of T with tb^2 for small t_b can be obtained if tunneling is treated as a perturbation to lowest order. Eventually, for higher values of the hopping of the barrier, the transmission goes up to T=1.

We also can study the resonant tunnel effect in a system with a double barrier. The barriers are represented with a black hopping (t_b) in Figure 2.13 (b) with a different value from the hopping in chain, in this case $t_b = 0.2t$. We calculate the transmission probability as a function of the number of sites of the chain inside of the barriers.

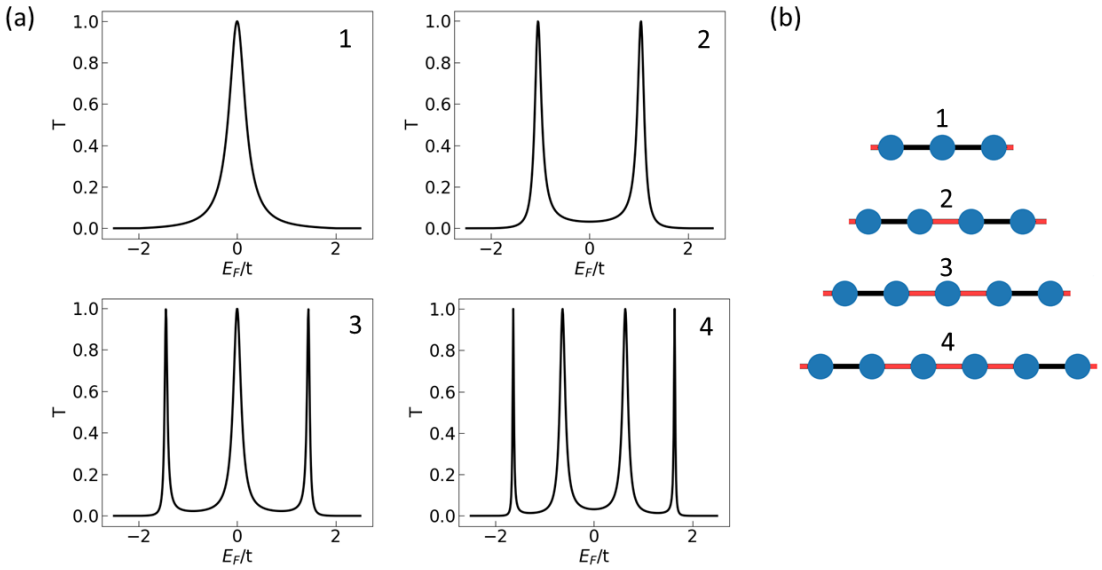

Figure 2.13: (a) Transmission probability for chains with a double barrier as a function of the energy for different lengths. (b) Schematic representation of hopping between the atoms in a chain in red and in black a hopping with a lower value acting as a barrier.

As seen from the results 2.13 (a), the number of resonances in which the system is able to conduct match the number of atoms that form the chain. In chains with an odd number of atoms a peak is present at $E_F = 0$. All the resonances achieve T=1.

The hopping value of the barrier is also an important quantity to the shape of the resonance. We compute the conductance for a system with a single site between the two barriers (see Figure 2.13 (b.1)).

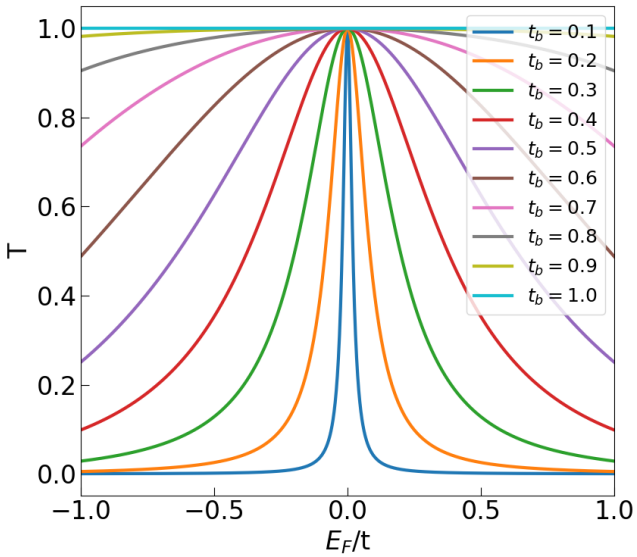

Figure 2.14: (a) Transmission probability in a double barrier for different values of the barrier hopping value.

As t_b is increased, the T goes from the resonant tunneling regime to the perfect conductance regime ($t_b = t$). The width of the resonant tunneling curve increases with the hopping value of the barrier.

2.4.2 Examples with graphene nanoribbons

The device atomic positions are previously generated and imported to Kwant. We generate a thin slice of graphene that match the width of the device using a honeycomb lattice. With this, we ensure that the leads generated by the same honeycomb lattice can find the places to attach it. Hopping are set between all the parts for Kwant to generate the tight binding Hamiltonians and calculate the transmission from the scattering matrix.

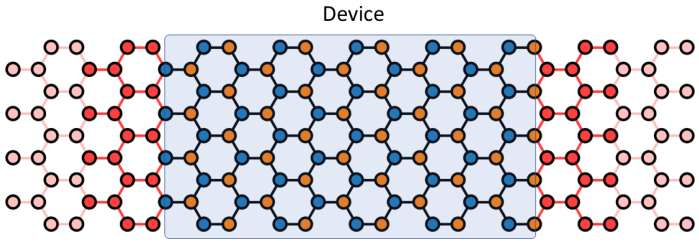

Figure 2.15: Schematic representation of the device embedded between the right and left graphene electrodes forming a semi-infinite system.

We can test the software with two giving system formed by a zigzag GNR with N=30 and an armchair edge one with N=50 with no constrictions:

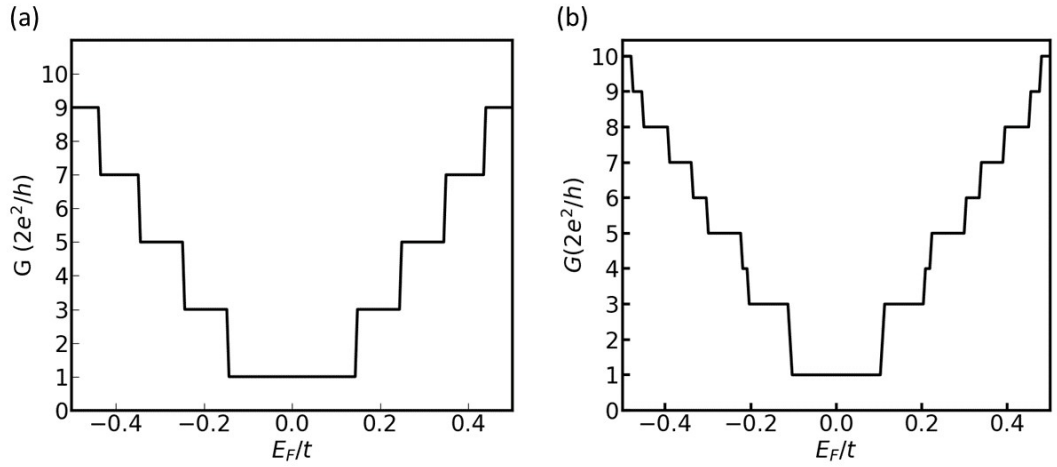

Figure 2.16: Conductance as a function of the energy in terms of the hopping value for a device without constriction in a system with (a) zigzag edges with N=30 and (b) armchair edges with N=50.

As we can see from the Figure 2.16, we obtain a quantum of conductance near the Dirac point. As we increase the Fermi energy the conductance goes up in multiples of G_0, as expected.

Chapter 3

Results

3.1 Single atomic constrictions in graphene electrodes

In this chapter we are going to present the results of the theoretical study of the conductance in nanocontacts between graphene electrodes as a function of various characteristics of the system. We will consider the width of both electrodes and constriction and the conductance as a function of the Fermi energy. We will study also the difference between the tight binding model considering nearest neighbours and third nearest neighbour contribution.

The hopping term, in the tight binding model, will be a constant value as mentioned before in section 2.1. Although it is possible to take the value from first principles calculation or experimental data [45, 54, 55], we normalize the energy to the hopping, so the results are independent from this value. In some cases, we obtain conductance values under $10^{-10}\,G_0$. These are, for all practical purposes, equivalent to zero. The widths of the ribbons ($W_R(N)$) will follow the definition presented in 2.1.2 for each type of edge.

The value of the conductance will be obtained as the averaged value around the Dirac point ($E_F = 0$) within a window of energies ($-\Delta E$, ΔE) where $\Delta E = 0.025\,t$:

$$G_{E_F=0} = \frac{1}{2\Delta E}\int_{-\Delta E}^{\Delta E} G(E)dE \tag{3.1.1}$$

Following this procedure, we make sure that we have realistic results, since it is not possible to achieve perfect zero temperature.

3.1.1 Conductance through a single atomic contact between graphene ribbons as a function of the electrodes width

One possibility to achieve a single contact between two graphene nanoribbons is to approach the graphene sheets with a certain angle. See for instance Figure 1.4 (a) and reference [40]. In order to emulate this geometry in the plain, we simply make the hopping value in the middle of the device zero along the finite direction. The one atomic contact position is set with a normal hopping between the two atoms from both electrodes. It is modeled to be at the center of the ribbons, though not all the systems will allow it.

3.1.1.1 Zigzag

To start, we perform the calculation of the conductance using zigzag electrodes through a single carbon-carbon contact as seen in the schematic representation of the device in Figure 3.2 (a). We are going to obtain the conductance as a function of the Fermi energy (G(E)) for a given width, in this case N=30.

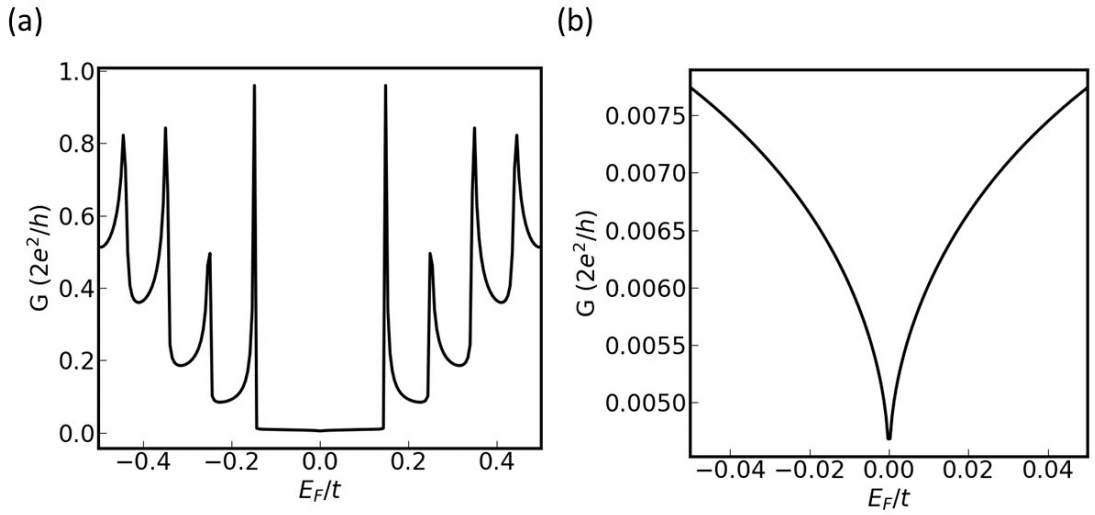

Figure 3.1: (a) Conductance as a function of the Fermi energy for a given system simulating a single contact between zigzag edge electrodes with N = 30. (b) Zoom at the conductance near Dirac point.

Taking a look to the graph 3.1 (a), for a range of energies between $(-0.5, 0.5)t$, we can observe that the system with the atomic-sized constriction presents a wide gap followed by sharp peaks at different energies that correspond to different resonances, some of them are able to get near the quantum of conductance. However, in 3.1 (b), the value of conductance drops to zero at exactly $E_F = 0$.

Next, we analyze how the conductance changes near the Dirac point by taking the mean value of G in a window of energy $(-0.025t, 0.025t)$ for different widths of the electrodes. We are going to test the widths $(W_R(N))$ in range from N=5 to N=75.

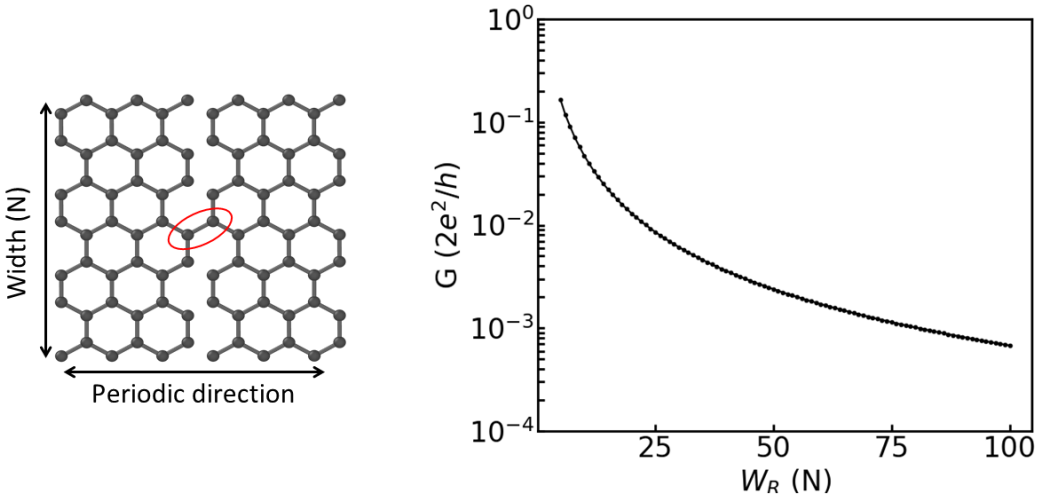

Figure 3.2: (a) Schematic representation of single contact (marked with a red circle to highlight the atomic contact) between two zigzag nanoribbons. (b) Conductance, averaged around the Dirac point, as a function of the width of the graphene electrodes.

As seen in Figure 3.2 (b) we find that for widths under N=20 the values of the conductance are an order of magnitude below the quantum of conductance and from there it tends to decrease with the width of the ribbon. Close to $E_F = 0$, the only bands contributing to transport are the edge states. Their wave functions peak at the edges and decay in the middle of the ribbon, where the nanocontact is placed. As a result, as the width increases, the weight of the edge state on the contact decreases, explaining the $G(W_R)$ curve that we obtain. In the macroscopic limit, the single atom conductance will be essentially zero. This behaviour is very different from the case of conventional conductors.

3.1.1.2 Armchair

In the case of armchair edge, we focus only on the gapless ribbons, as seen in 2.1.2. Following the schematic example of the device presented in Figure 3.4 (a), we compute the conductance as a function of the Fermi energy.

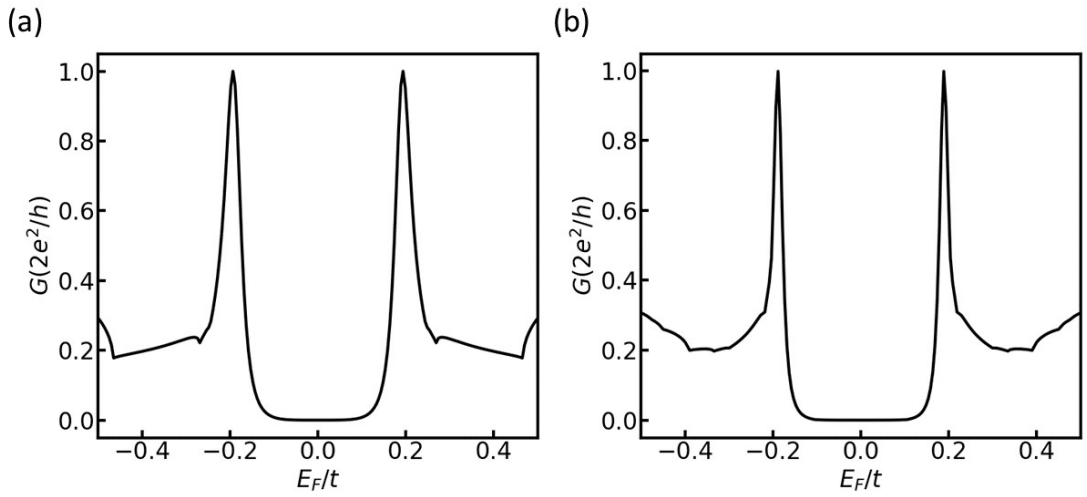

Figure 3.3: Conductance as a function of the energy in terms of hopping for a system simulating a single contact between armchair edge electrodes with (a) N = 14 and (b) N = 50.

The graph shows a wide gap and resonances that are able to reach the quantum of conductance for some energies in both cases. The single contact between the graphene nanoribbons make the system a semiconductor with a noticeable gap, far from the metallic behavior of the ribbons.

We calculate the conductance as a function of the widths of the electrodes in a range that goes from N=5 to N=98.

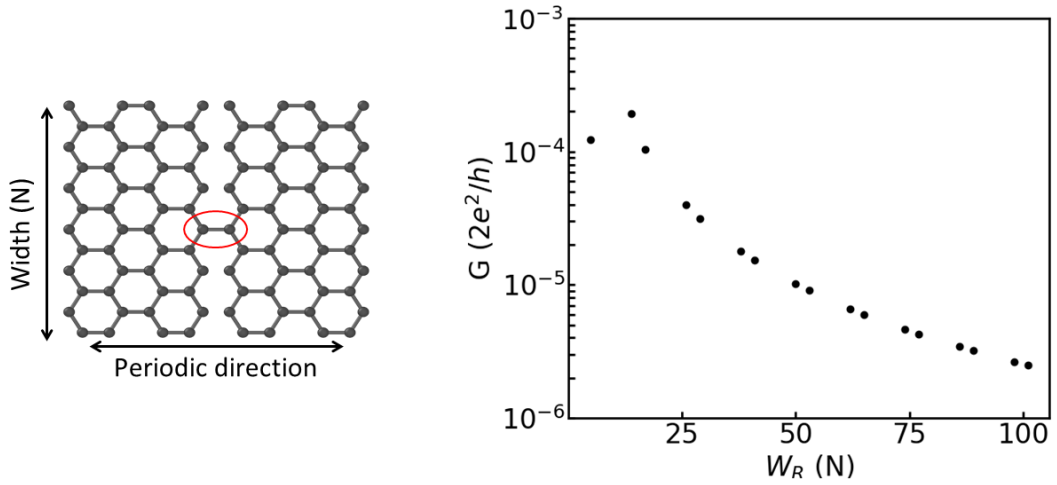

Figure 3.4: (a) Schematic representation of single contact (marked with a red circle) between two armchair nanoribbons. (b) Conductance averaged around the Dirac point as a function of the width of the graphene electrodes near the Dirac Point.

In the graph 3.4 (b), the conductance drops when the system increase its size. The trend is similar to the electrodes with zigzag edges (Figure 3.2 (b)), however the values are several orders of magnitude lower as the values around the Dirac point are almost negligible due to the lack of edge states.

3.1.2 Conductance through a nanocontact between graphene electrodes as a function of the constriction width

Up to now, we have seen that for a single carbon-carbon bond the device does not show the metallic behavior originally presented in ribbons. The size of the ribbons became almost irrelevant for the conduction from a certain width. The next step is to see how the constriction widths affect the conduction for certain electrode sizes. Hence, we selected a few ribbons with different widths to perform the calculations within a range of constriction widths (W_c).

The methodology followed is based on adding one contact at the time between the graphene sheets until obtaining the complete ribbon. This situation could be similar to a experimental wedge break. We simulate this by making each hopping value, in a vertical section of the device, zero for each contact. The filling can be carried out in two ways, from the center to the sides or from edge to edge. We choose edge to edge for simplicity since important differences where not observed.

3.1.2.1 Zigzag

We measure the conductance near the Dirac point for every contact added in the constriction as shown in Figure 3.5 (a) for the electrodes with size N = 15, 30. The constriction width is expressed as a function of the number of contacts between the ribbons ($W_R(N)$). For the zigzag edge, the number of bonds is the same as N, which defines the width of the electrodes.

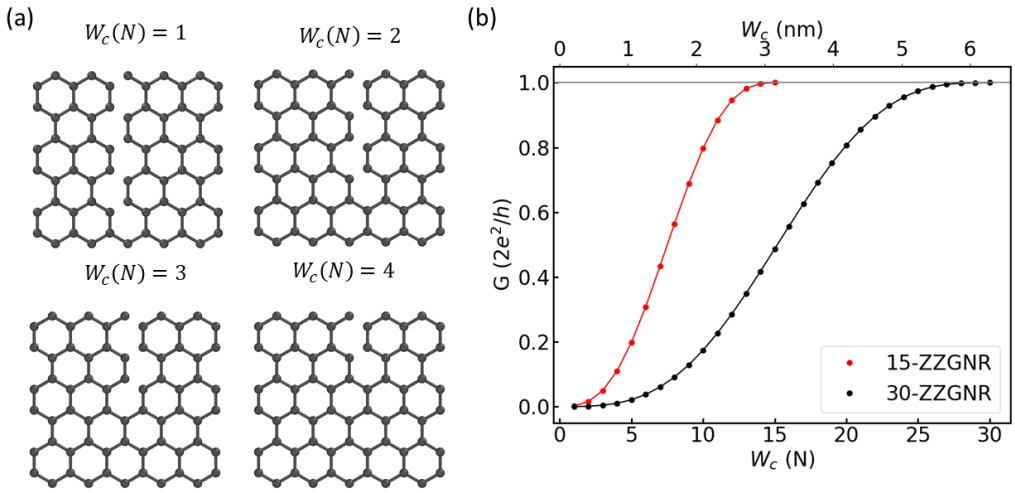

Figure 3.5: (a) Representation of the contact between two zigzag electrodes. The number of bonds will increase as depicted in the images with the increase of N, thus changing the width of the constriction. (b) Conductance as a function of the constriction width $W_c(N)$, averaged around $E_F = 0$ with N = 15, 30.

The graph 3.5 (b) shows a continuous increment on the conduction with each new bond made between the electrodes. It is not until the last bond is made, making $W_c = W_R$, that we get the quantum of conductance at the neutrality charge point. On the other hand, we can make the consideration of being a conductor in the scenarios where the system shows at least $G = 0.1\,G_0$. In the case of N=15, the conduction goes over $0.1\,G_0$ with $W_c = 4$ and for N=30, we get the same level of conductance with $W_c = 8$. The same happens for all the values until the system reaches $1G_0$, thus we can see that there is a relation between the widths of the electrodes and the constriction.

3.1.2.2 Armchair

We now consider transport across a series of contacts of increasing width W_c, between two graphene ribbons with armchair termination. In Figure 3.6 (b) we show $G(W_c)$ for two ribbons of different width, N=29 and N=35. The filling of the ribbon is performed in an analogous way to the zigzag geometry. The number of possible contacts that can be made in an armchair edge electrode corresponds to half the N of the widths in the ribbon.

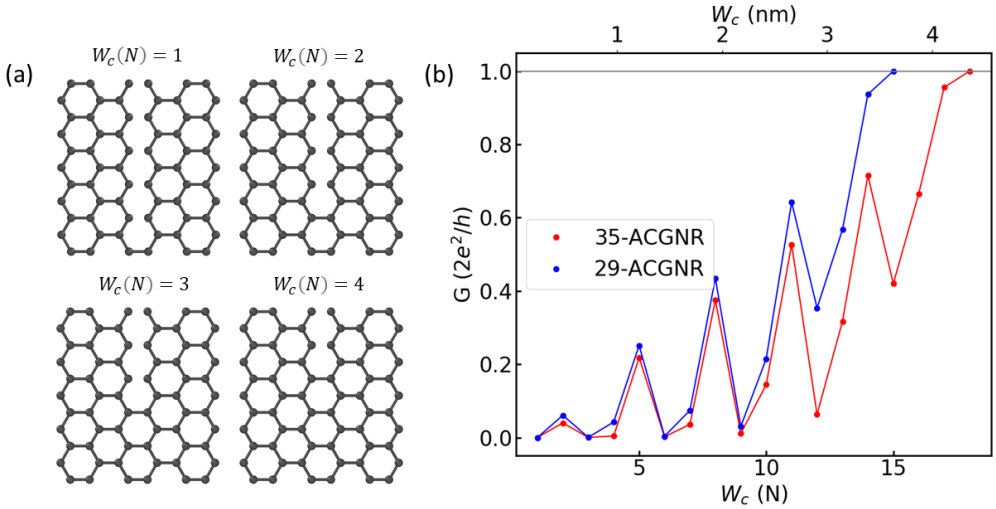

Figure 3.6: (a) Schematic representation of the constriction for different widths. (b) Conductance as a function of the number of contacts, related to the constriction width $W_c(N)$ averaging around $E_F = 0$ with N = 29, 35.

In armchair based electrodes, the conduction grows presenting peaks at certain constriction widths ($W_c = 2, 5, 8, 11, ...$). These peaks appear every three integer values of the constriction width, following the same rule to determine the armchair ribbons with a metallic behavior (see 2.1.2). Also, we can observe in Figure 3.6 (b) a relation between W_R and W_c, since in order to achieve a certain value of conductance, the number of the contacts necessary varies proportionally to the width of the electrodes.

To test this idea, we compute the conductance in much wider armchair ribbons using only the integer values of constriction widths that presents higher peaks in the conduction (Figure 3.6 (b))in this edge type to simplify the calculations. The calculus was performed with a specific Fermi energy, in this case $E_F/t = 0.1$, to eliminate all the possible variables. Results are presented in Figure 3.7.

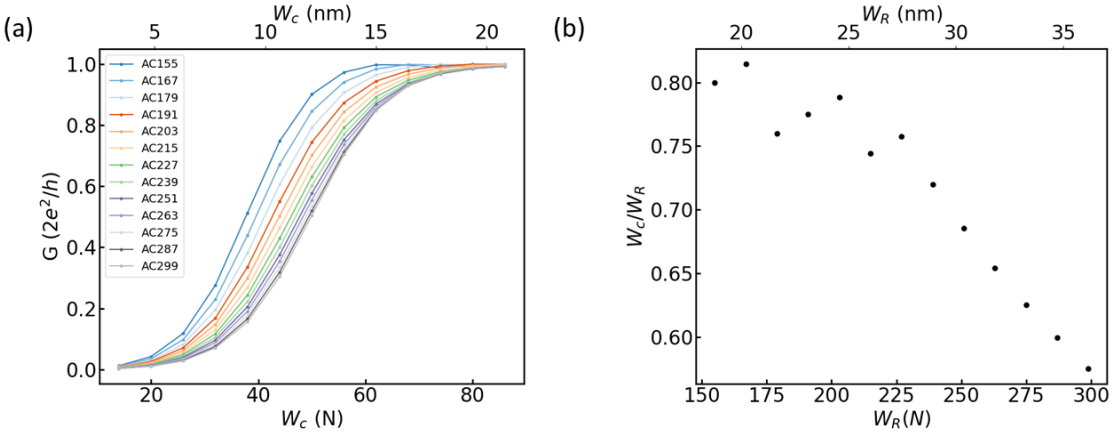

Figure 3.7: (a) Conductance as a function of the constriction width. (b) Relation between the width of the nanoribbons and their constriction to obtain 1 G_0.

From the results shown we can deduce that there is not a preferential relation between ribbons widths and constriction size. As we can observe in the graph 3.7 (a), with $W_c(N)$ around 75-80 bonds we can recover the quantum of conductance, reaching a constant value for bigger systems. In graph 3.7 (b), we can observe the behavior mentioned as a drop in the relation between size of the ribbon and width of the constriction to achieve a quantum of conductance.

3.1.3 Conductance away from the Dirac point

From the results of a single contact (see 3.1), we have seen that, for sufficiently wide ribbons, atomic scale nanocontacts have a vanishing conductance as long as the Fermi energy is in an energy window of several tens of meV around the Fermi energy. Effectively, there is a gap for the transmission.

This is very different from the behaviour of a normal conductor. In this section we recover the conventional behavior of atomic scale contacts between normal metals by looking at the behaviour of conductance for $E_F = t$, where many channels are available at the electrodes, and the density of states is no longer dominated by the Dirac bands.

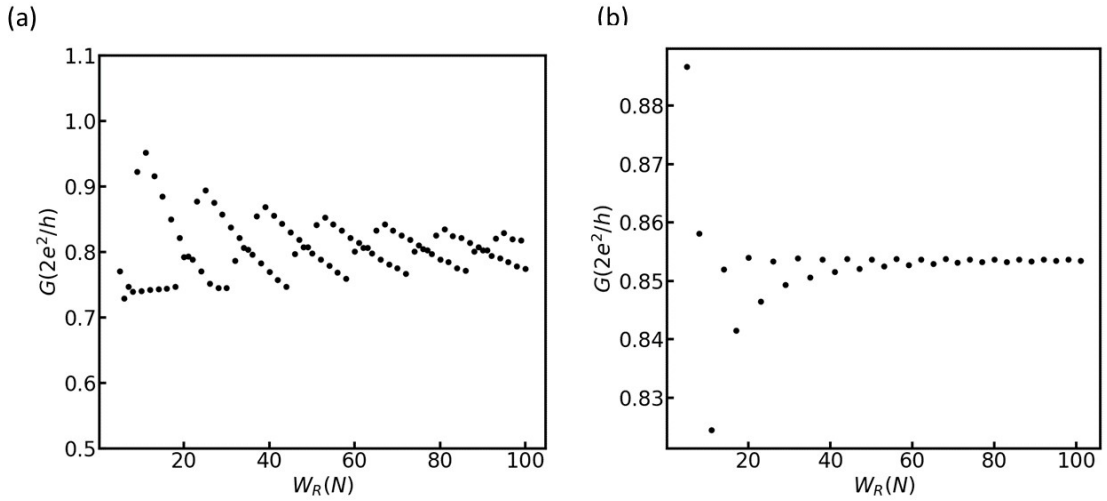

Figure 3.8: Measurements of conductance for different sizes of ribbon averaged around $E_F = t$ for both (a) zigzag and (b) armchair through a single contact.

From the results obtained in Figure 3.8 (a), we can deduce that for bigger widths of zigzag ribbons, the conduction starts to stabilize and the value is in the order of a quantum of conductance, approximately at $0.8\,G_0$. In the case of armchair (Figure 3.8 (b)) the conduction obtained rapidly reaches a constant value, being $G \approx 0.84\,G_0$. This shows that even for a single contact between the graphene nanoribbons, the metallic behavior presented in the ribbons without constriction is recovered for energies similar to the hopping term.

3.1.4 Third nearest neighbors contribution

As seen in section 2.1.3, in order to implement a more realistic model, we can take in consideration the contribution of third nearest neighbors in the system. The hopping term for the third neighbours is $t_3 = 0.15t$, changing slightly the band structure of the ribbons as seen in Figures 2.10 and 2.11. Now we will discuss how this affects the conductance through the single contact constriction.

3.1.4.1 Zigzag

In order to introduce the third nearest neighbours in the system, we added hopping values to the atoms in the constriction between the electrodes but only the closest to the the single atomic contact as it is presented in Figure 3.9 (a). We performed a calculation of the conductance value as a function of the widths of the electrodes (Figure 3.9 (b)).

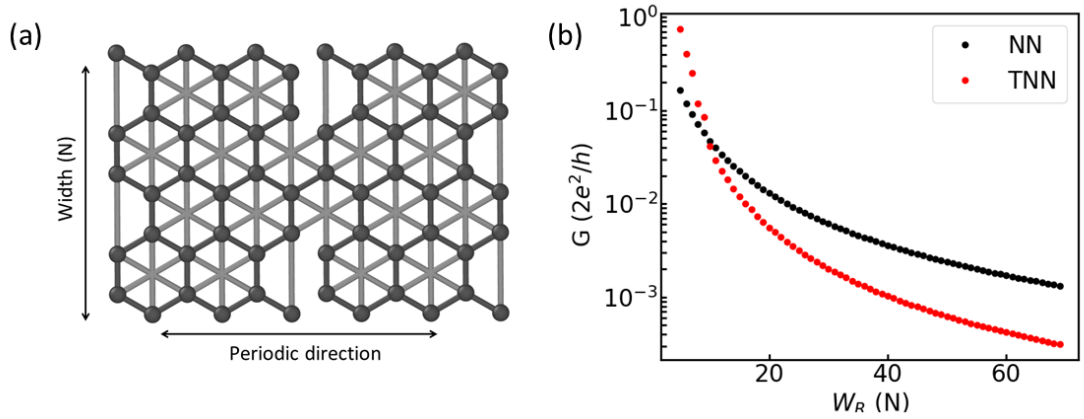

Figure 3.9: (a) Single contact between two zigzag sheets of nanoribbon with visual representation of third nearest neighbours. (b) Comparison of the conductance as a function of the electrode width averaged around the Dirac point between the model considering only nearest (NN) and third nearest (TNN) neighbours contribution.

For electrodes with smaller widths, the conduction is better with the third neighbour contributions as the number of channels is higher. On the other hand, for bigger sizes from $W_R(N) = 10$, acts contrary, lowering down an order of magnitude the conductance obtained in the nearest neighbours model. Although, there is a noticeable discrepancy between the two approximations, the conclusions are the same with both models. The conductance of this type of contacts are far from the metallic behavior.

3.1.4.2 Armchair

Analogous to the calculation with the zigzag edge, we will add the hopping of the third nearest neighbour closest to the nanocontact. This is presented in 3.10 (a).

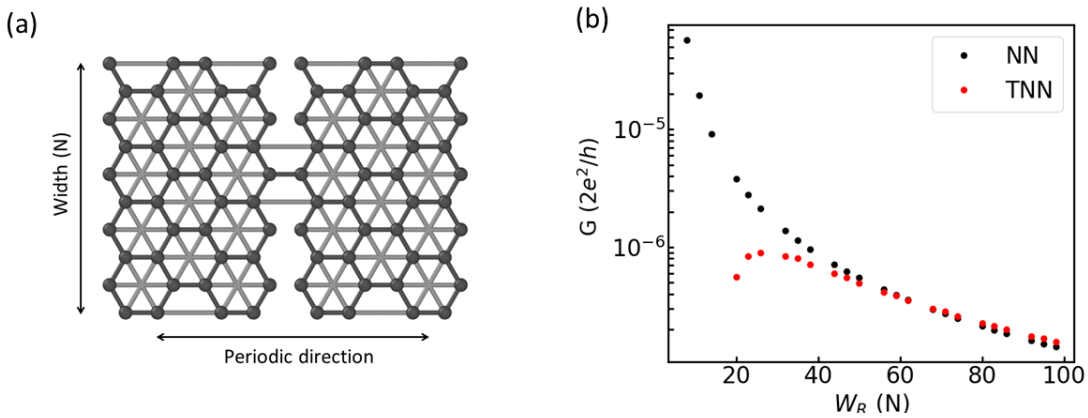

Figure 3.10: (a) Single contact between two armchair sheets of nanoribbon with visual representation of third nearest neighbours. (b) Comparison of the conduction as a function of the electrode width averaged around the Dirac point between the model considering only nearest (NN) and third nearest neighbours (TNN) contribution.

As is presented in Figure 3.10 (b), when looking at the conductance calculated using both methods, differences appear. The third nearest neighbour model shows lower values for smaller widths compared to the nearest neighbour model but at around $W_R(N) = 40$, the behavior became almost identical. This shows that the effect is visible when the edges are closer to the contact and the small gap that appears in the bands contribute to the resistance in the system. Although, this confirms that for bigger sizes, the results with only nearest neighbours are accurate enough.

3.1.5 Conduction as a function of W_c and E_F

We have seen that graphene nanocontacts made out of a single contact in between the electrodes is far from the quantum of conductance at $E_F = 0$, we have also seen that we can recover the metallic behavior by increasing the width of the constriction (W_c) or increasing the Fermi energy. In Figures 3.11 and 3.12 we sum up the results obtained as a relation of $G(E_F, W_c)$. We have selected ribbons with a considerable width because the values tends to stabilizes for bigger systems, as seen in the previous results.

3.1.5.1 Armchair

In the case of armchair edge, we have selected one system with the electrodes width of N=101 that have a metallic behavior. We have performed calculations of the conduction for the different possible constrictions widths and the energy of the system from the neutrality charge point to the hopping value.

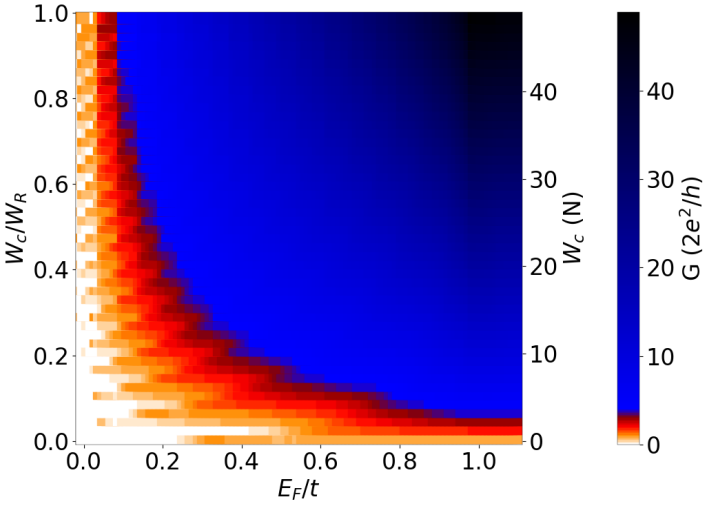

Figure 3.11: Conduction in terms of contacts between armchair electrodes with N=101 and the energy of the system. Reaching $E_F = t$ and $W_c = W_R$.

From the results presented in 3.11, we can deduce all the key points that we have seen so far. With a single contact and the Fermi energy at neutrality charge point, the system presents a almost negligible conductance. When increasing the width of the constriction ($W_c = W_R$) we recover the quantum of conductance (marked as orange in the graph). If we increase the energy ($E_F = t$), eventually, we will recover the conduction as we cross more bands. We also found configurations, where we recover the metallic behavior with a certain combination of constriction width and Fermi energy. We can also see that for $E_F = t$, for each contact in the constriction we sum a G_0 to the total conduction.

3.1.5.2 Zigzag

In the case of zigzag electrodes, we selected $W_R(N) = 75$. We carried out the same analysis in Figure 3.12, as for armchair edge.

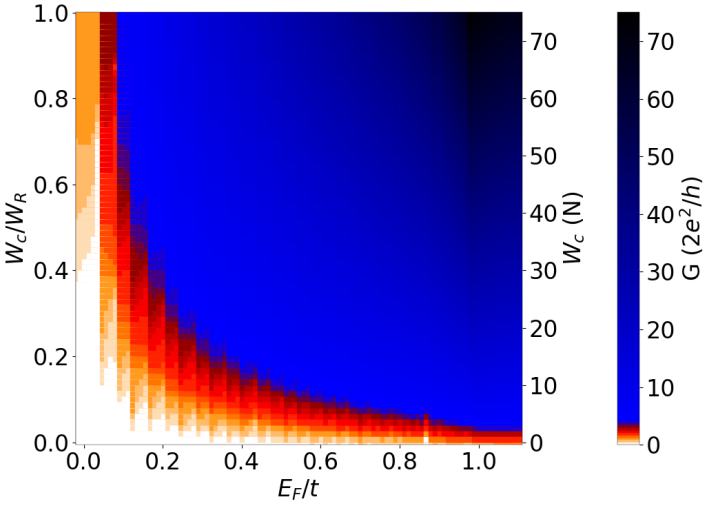

Figure 3.12: Conduction in terms of contacts between zigzag electrodes with N=75 and the energy of the system. Reaching $E_F/t = 1$ and $W_c = W_R$.

From the graph we deduce that the results are similar to the armchair edge ones. At the limits $W_c = W_R$ and $E_F = t$, the metallic behavior of the system without constriction is recovered. Also, the conductance is quantized in multiples of G_0 by the number of contacts in the constriction.

And so, we conclude that single contact constrictions between graphene electrodes change the system from a zero gap semiconductor for the uninterrupted ribbon to a semiconductor with a noticeable gap. We are able to recover the metallic behavior when applying the limits of energy and width of the constriction.There are intermediate solutions that may be interesting to develop specific devices.

3.2 Different type of geometries as constrictions

Apart from the simplest constriction that we have been studying, other types of contacts were also tested. In this chapter we are going to focus on two of them: triangular shape constrictions in armchair edges and carbon atomic chains as a function of the number of atoms in it. We also attempt to introduce the angle between the graphene electrodes in the model using a simple approximation.

3.2.1 Triangulenes

We introduce a triangular shape constriction in the electrodes, forming a triangulene. We put in contact the tip of the triangulenes to make a nanometric junction. We will define the width by the number of hexagons in the base (Figure 3.13). Although, this geometry naturally shapes to a single point of contact The results of single contact have

been discarded, the conductance calculated was under the numerical error for all the electrodes widths tested. we will study a double contact between them as represented on of Figure 3.14 (a).

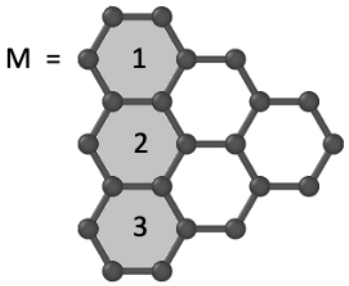

Figure 3.13: Schematic representations of a triangulene with a base M=3.

Following the same scheme used in the approach to single contact calculations, we measure the conductance near zero energy, taking a averaged values of conductance around the Dirac point as a function of the triangulenes base size. This time, we tested two types of contacts, single and double contact between the triangulenes.

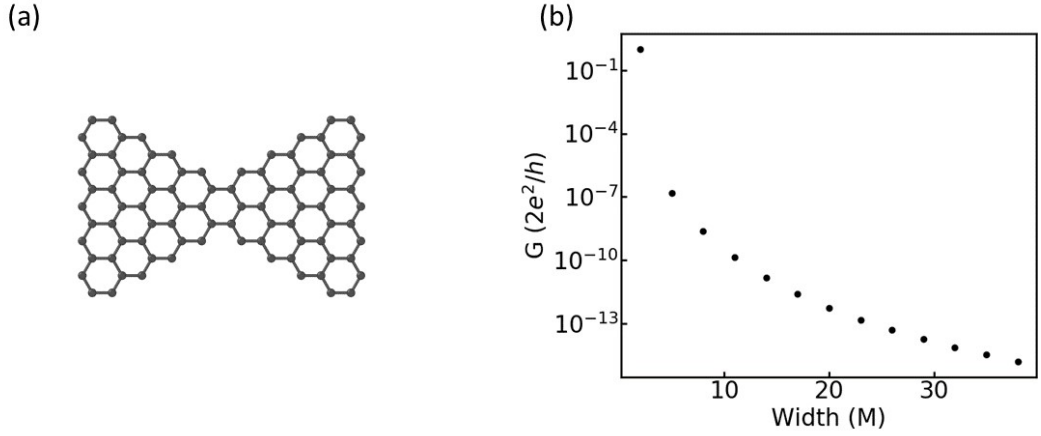

Figure 3.14: (a) schematic example of a double contact for triangular shape constrictions. (b) Conductance averaged around the Dirac as a function of the triangulene base size.

From Figure 3.14 the conductance values are almost negligible. Reducing the conductance with the size, following the same pattern as for a simple single contact between graphene electrodes. We also tested the third neighbour contribution in this geometries. The hopping values is the same as in previous sections. In this case, as seen in the top of Figure 3.15 (a), we include the single contact.

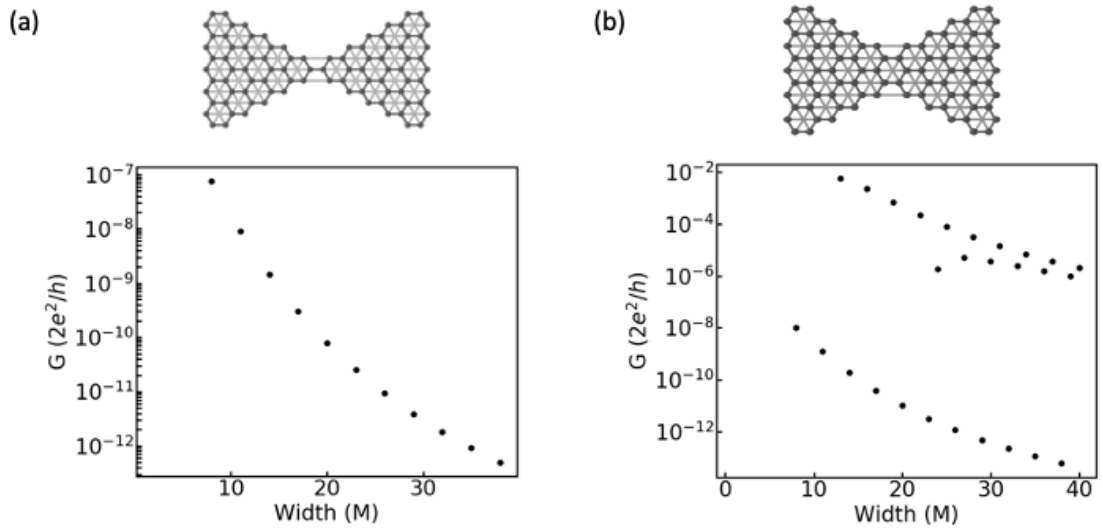

Figure 3.15: (a) schematic example of the single contact for triangular shape constrictions with a visual representation of third nearest neighbours hopping in the upper part and the conductance values averaged around the Dirac point as a function of the triangulene base size. In (b), following the shame scheme for a double contact.

From the graphs in Figure 3.15 we confirm that extremely small constrictions in triangular shape contacts between graphene electrodes are not able to conduct at E=0 as a metallic nanocontact would. Similar systems were already tested for wider constrictions showing similar results [56].

Last, we calculate the conduction as a function of the Fermi energy using the same triangulene size (M=25) for all the four types of contacts tested. Single (1-NN) and double contact (2-NN) with nearest neighbour contribution and single (1-TN) and double contact (2-TN) with third nearest neighbour contribution taken into account.

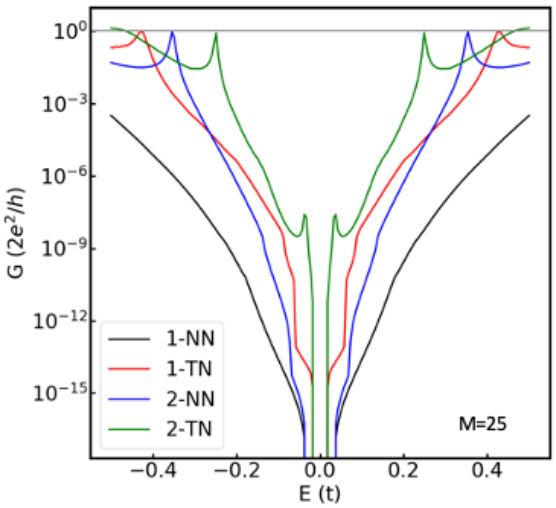

Figure 3.16: Conductance as a function of the energy for system with a triangulene M=25 at the tip with different types of contacts.

In the graph 3.16 we found that all of them show a gap. Systems with third nearest neighbours contribution, and therefore, having more channels (1-TN, 2-TN), have a smaller gap. The metallic behavior is recover in all of them, again, being the number of channel in each one, key to the energy needed to get a quantum of conductance. 1-NN, only having a single channel recover the quantum of conductance around $E_F = t$, outside of the range shown.

3.2.2 Angle between electrodes

As mention in the introduction, in a previous work [40], in order to achieve the single contact between the graphene nanoribbons, they have to approach them in a certain angle. In order to tackle this situation we made the attempt to model this scenario by modulating the hopping term in the junction. This approximation was made under the Slater-Koster interatomic matrix elements [57]. Those give information about the relation between the different orbitals between atoms. In this case, we consider that only the difference in the alignment of the p_z orbitals contribute the most part of the total change in the system, particularly for lower energies, being other options more energy cost for electrons to move. Therefore, the relation with the angle between the planes, taking into consideration those assumptions, can be written as follow:

$$t_\theta = t \cdot cos(\theta) \tag{3.2.1}$$

being θ the angle for from the junction between the two graphene planes.

We introduce a variable hopping for the single contact as shown in Figure 3.17 (a) and we measure the conductance as a function of the angle.

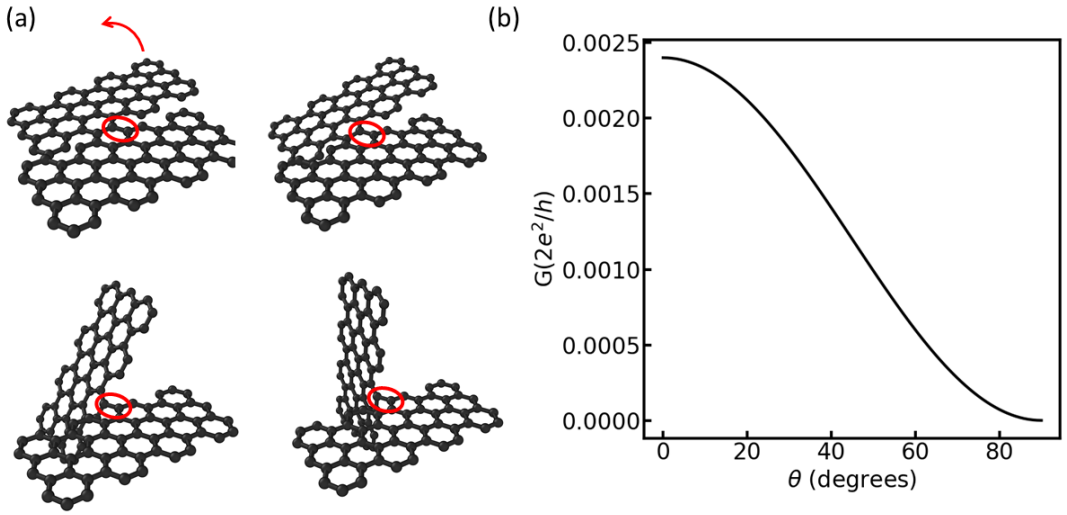

Figure 3.17: (a) Schematic representation of the rotation between two graphene electrodes with a single contact at different angles. (b) Conduction for a single contact averaged around the Dirac point as a function of the angle between the graphene electrodes for zigzag edge with N=50.

As seen in graph 3.17 (b), the change in conduction follows the cosine function with no sudden changes in the zigzag geometry. The armchair results, being almost negligible with angle zero, does not improve therefore the numbers are below the possible numerical error of the calculations and it is not shown here.

3.2.3 Carbon atomic chains as contacts

After the type of contacts tested in this work, we decided to take a glance on what the behavior should be for carbon atomic chains. Taking into account that the model is simplistic for this type of structures. The reason to try this contact is the existence of evidence of formation of chains when the graphene electrodes are retracted [40].

The device consist on adding carbon atoms between the graphene ribbons, maintaining the same hopping values present on the electrodes. In the case of armchair edges, the result shows almost similar or worst values of the averaged conductance near the Dirac point than the system with the single contact for any type of atomic carbon chain study.

Therefore, we tested the zigzag ribbons, and as we are going to see, differentiating between the atomic chains formed by an even or an odd number of carbons.

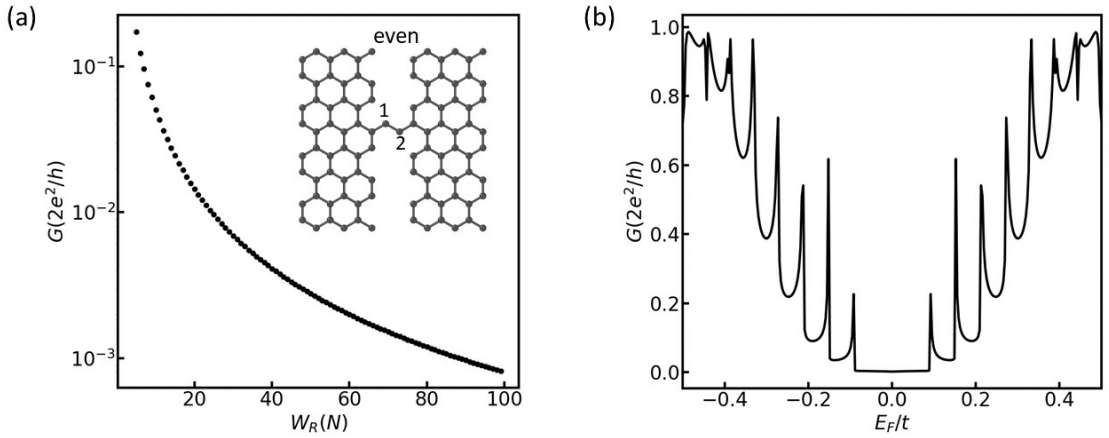

Figure 3.18: (a) Conductance as a function of the ribbon widths averaged around the Dirac point for even carbon atomic chains as contact.(b) G(E) for the the double atom chain contact, for a ribbon width N=50.

From Figure 3.18 (a) we concluded that for a carbon chain formed by an even number of atoms, the conductance averaged around the Dirac point is similar to the single contact case. In Figure 3.18 (b) we can see that the example with N=50 presents a conductance that drops when reaching $E_F = 0$ surrounded by resonances.

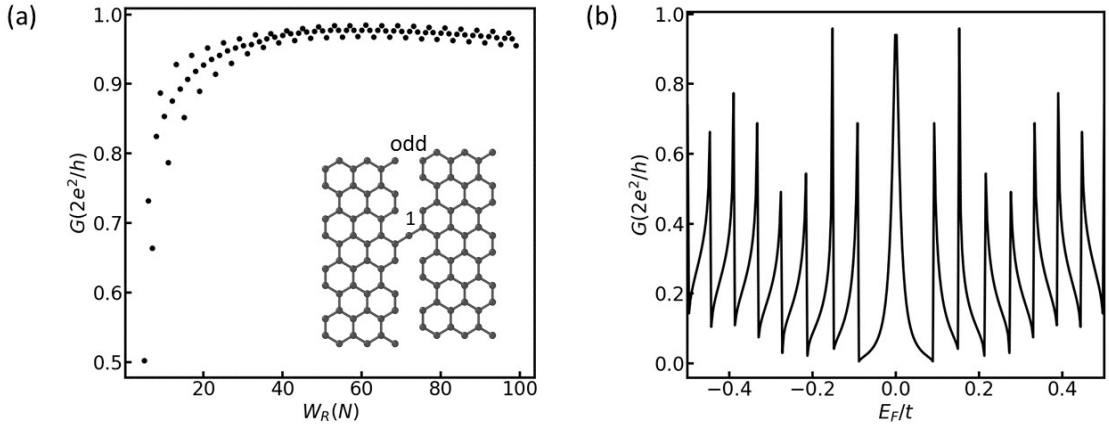

Figure 3.19: (a) Conductance as a function of the ribbon widths averaged around the Dirac point for even carbon atomic chains as contact.(b) G(E) for the the single atom chain contact, for a ribbon width N=50.

For zigzag edge electrodes with an odd number of carbon atoms forming the chain the averaged conductance around the Dirac point presents values in the same order of magnitude that the quantum of conductance. In the system with electrodes N=50, we can see that a sharp peak appears at zero Fermi energy, in the Dirac point, recovering the metallic behavior.

This can be explained by the resonant tunnelling effect in system with a double barrier. Being the resonance formed by the stationary wave inside the two barriers following the

example of monoatomic chain in section 2.4.1. In our case, the exponential decay of the zigzag edges makes the effective hopping to the carbon chain in the contact small, acting effectively as a barrier.

Chapter 4

Discussion and conclusions

In this work, we have studied the conductance of atomic-sized graphene nanocontacts. For that matter we have used the tight binding approximation to nearest-neighbours and third nearest-neighbours applying Green functions technique and the Landauer formula.

We have studied thoroughly the conductance as a function of the geometry of the contact and the graphene electrodes.

During our work, we have neglected electron-electron interactions. This may be a serious problem in the case of the zigzag edge states, where interactions lead to magnetism and change the dispersion energy of the zigzag states [58]. This may be less of a problem as temperature depletes edge magnetism. Likewise, electron-electron interactions may also play a role in the case of resonant transport across the single atom chains. In such system, Coulomb blockade effects are to be expected, or perhaps even Kondo effect.

A four orbital tight binding model should be used to described transport connecting two non-coplanar graphene electrodes. It is also necessary to implement a more complete model of an atomic carbon chain as the one used is missing many of the key features of these structures.

We have found that the conductance of two semi-infinite 2D graphene planes connected by an atomic scale contact vanishes as long as the Fermi energy is not very far from the Dirac point. Moreover, we studied how to recover the metallic behavior of the system. Our theoretical results show the role of the size of the constriction and the Fermi energy. We have demonstrated that by tuning these two variables, we can obtain configurations with conductance values near G_0.

Different kind of constrictions were tested between graphene electrodes. In the case of triangular shape constrictions applied to armchair edge electrodes, we have also found a system that is not able to conduct near the neutrality charge point. For smaller widths, the edge states have a mayor contribution but when the size increase, the value of conductance drops, similar to the single atomic contact constriction.

Moreover we have modeled the hopping term in the nanocontact to emulate a rotation of the graphene electrodes with a single contact and we have measured the conductance as a function of the angle. We have observed a measurable decrease of the conductance for the case of zigzag edge electrodes and an almost negligible change for armchair ribbons.

Finally, we have studied carbon atomic chains between two electrodes in the scenarios of zigzag and armchair edge. As summary, we have found that for the case of armchair geometry the results are similar to the ones observed in single atomic contact systems. However, for zigzag edges electrodes, the conductance is close to the quantum of conductance when the chain is formed by an odd number of carbon atoms. This last result is explained by a quantum tunneling effect in a system with a double barrier, similar to the case of a monoatomic chain discussed in the present work.

Bibliography

[1] Sabina Caneva, Pascal Gehring, Víctor García-Suárez, A. Garcia-Fuente, Davide Stefani, Ignacio Olavarria, Jaime Ferrer, Cees Dekker, and Herre Zant. Mechanically controlled quantum interference in graphene break junctions. *Nature Nanotechnology*, 13, 12 2018.

[2] Sabina Caneva, Matthijs D. Hermans, Martin Lee, Amador Garcia-Fuente, Kenji Watanabe, Takashi Taniguchi, Cees Dekker, Jaime Ferrer, Herre S. J. van der Zant, and Pascal Gehring. A mechanically tunable quantum dot in a graphene break junction, 2020.

[3] P. Drude. Zur elektronentheorie der metalle. *Annalen der Physik*, 306(3):566–613, 1900.

[4] Amogh Kinikar, Twarakavi Sai, Semonti Bhattacharyya, Adhip Agarwala, Tathagata Biswas, Sanjoy Sarker, H. Krishnamurthy, Manish Jain, Vijay Shenoy, and Arindam Ghosh. Quantized edge modes in atomic-scale point contacts in graphene. *Nature nanotechnology*, 04 2017.

[5] G. E. Moore. Cramming more components onto integrated circuits, reprinted from electronics, volume 38, number 8, april 19, 1965, pp.114 ff. *IEEE Solid-State Circuits Society Newsletter*, 11(3):33–35, 2006.

[6] Transistor count trends. https://www.design-reuse.com/news/47652/transistor-count-trends.html.

[7] Richard P. Feynman. There's plenty of room at the bottom. 1959.

[8] N.W. Ashcroft and N.D. Mermin. *Solid State Physics*. HRW international editions. Holt, Rinehart and Winston, 1976.

[9] J.C. Cuevas and E. Scheer. *Molecular Electronics: An Introduction to Theory and Experiment*. EBSCO ebook academic collection. World Scientific Publishing Company Pte Limited, 2010.

[10] J. C. Cuevas, A. Levy Yeyati, A. Martín-Rodero, G. Rubio Bollinger, C. Untiedt, and N. Agraït. Evolution of conducting channels in metallic atomic contacts under elastic deformation. *Phys. Rev. Lett.*, 81:2990–2993, Oct 1998.

[11] N. Agraït, J. G. Rodrigo, and S. Vieira. Conductance steps and quantization in atomic-size contacts. *Phys. Rev. B*, 47:12345–12348, May 1993.

[12] J. I. Pascual, J. Méndez, J. Gómez-Herrero, A. M. Baró, N. García, and Vu Thien Binh. Quantum contact in gold nanostructures by scanning tunneling microscopy. *Phys. Rev. Lett.*, 71:1852–1855, Sep 1993.

[13] C.J. Muller, J.M. van Ruitenbeek, and L.J. de Jongh. Experimental observation of the transition from weak link to tunnel junction. *Physica C: Superconductivity*, 191(3):485 – 504, 1992.

[14] J. K. Gimzewski and R. Möller. Transition from the tunneling regime to point contact studied using scanning tunneling microscopy. *Phys. Rev. B*, 36:1284–1287, Jul 1987.

[15] Nicolás Agra˙ Quantum properties of atomic-sized conductors. *Physics Reports*, 377(2):81 – 279, 2003.

[16] K. S. Novoselov. Electric field effect in atomically thin carbon films. *Science*, 306(5696):666–669, Oct 2004.

[17] R. Peierls. Quelques propriétés typiques des corps solides. *Annales de l'institut Henri Poincaré*, 5(3):177–222, 1935.

[18] Lev Davidovich Landau. The theory of phase transformations ii. *Phys. Z. Soviet Union*, 11(545):26–35, 1937.

[19] H.P. Boehm, A. Clauss, G.O. Fischer, and U. Hofmann. *Surface properties of extremely thin graphite lamellae*, volume 1, pages 73–80. 12 1962.

[20] Changgu Lee, Xiaoding Wei, Jeffrey W. Kysar, and James Hone. Measurement of the elastic properties and intrinsic strength of monolayer graphene. *Science*, 321(5887):385–388, 2008.

[21] Alexander A. Balandin, Suchismita Ghosh, Wenzhong Bao, Irene Calizo, Desalegne Teweldebrhan, Feng Miao, and Chun Ning Lau. Superior thermal conductivity of single-layer graphene. *Nano Letters*, 8(3):902–907, 2008. PMID: 18284217.

[22] A. Geim and K.S. Novoselov. The rise of graphene. *Nature materials*, 6:183–91, 04 2007.

[23] K. S. Novoselov, A. K. Geim, S. V. Morozov, D. Jiang, M. I. Katsnelson, I. V. Grigorieva, S. V. Dubonos, and A. A. Firsov. Two-dimensional gas of massless dirac fermions in graphene. *Nature*, 438(7065):197–200, Nov 2005.

[24] K.M. Kadish and F. D'souza. *Handbook Of Carbon Nano Materials (Volumes 7-8)*. World Scientific Series On Carbon Nanoscience. World Scientific Publishing Company, 2015.

[25] The quantum theory of the electron. *Proceedings of the Royal Society of London. Series A, Containing Papers of a Mathematical and Physical Character*, 117(778):610–624, February 1928.

[26] Hai-Yao Deng and Katsunori Wakabayashi. Decomposition into propagating and evanescent modes of graphene ribbons. *Physical Review B*, 90(4):045402, 2014.

[27] Y.-W. Tan, Y. Zhang, K. Bolotin, Y. Zhao, S. Adam, E. H. Hwang, S. Das Sarma, H. L. Stormer, and P. Kim. Measurement of scattering rate and minimum conductivity in graphene. *Phys. Rev. Lett.*, 99:246803, Dec 2007.

[28] S. Das Sarma, Shaffique Adam, E. H. Hwang, and Enrico Rossi. Electronic transport in two-dimensional graphene. *Rev. Mod. Phys.*, 83:407–470, May 2011.

[29] J. Tworzydło, B. Trauzettel, M. Titov, A. Rycerz, and C. W. J. Beenakker. Sub-poissonian shot noise in graphene. *Phys. Rev. Lett.*, 96:246802, Jun 2006.

[30] MI Katsnelson. Zitterbewegung, chirality, and minimal conductivity in graphene. *The European Physical Journal B-Condensed Matter and Complex Systems*, 51(2):157–160, 2006.

[31] Kentaro Nomura and AH MacDonald. Quantum transport of massless dirac fermions. *Physical review letters*, 98(7):076602, 2007.

[32] P. M. Ostrovsky, I. V. Gornyi, and A. D. Mirlin. Electron transport in disordered graphene. *Phys. Rev. B*, 74:235443, Dec 2006.

[33] F Miao, S Wijeratne, Y Zhang, UC Coskun, W Bao, and CN Lau. Phase-coherent transport in graphene quantum billiards. *science*, 317(5844):1530–1533, 2007.

[34] MI Katsnelson, KS Novoselov, and AK Geim. Chiral tunnelling and the klein paradox in graphene. *Nature physics*, 2(9):620–625, 2006.

[35] Mikhail I. Katsnelson. Graphene: carbon in two dimensions. *Materials Today*, 10(1):20 – 27, 2007.

[36] J. H. Bardarson, J. Tworzydło, P. W. Brouwer, and C. W. J. Beenakker. One-parameter scaling at the dirac point in graphene. *Phys. Rev. Lett.*, 99:106801, Sep 2007.

[37] Yu-Ming Lin, Vasili Perebeinos, Zhihong Chen, and Phaedon Avouris. Electrical observation of subband formation in graphene nanoribbons. *Physical Review B*, 78(16), Oct 2008.

[38] J. Fernández-Rossier, J. J. Palacios, and L. Brey. Electronic structure of gated graphene and graphene ribbons. *Physical Review B*, 75(20), May 2007.

[39] N. M. R. Peres, A. H. Castro Neto, and F. Guinea. Conductance quantization in mesoscopic graphene. *Phys. Rev. B*, 73:195411, May 2006.

[40] Amedeo Bellunato, Sasha D. Vrbica, Carlos Sabater, Erik W. de Vos, Remko Fermin, Kirsten N. Kanneworff, Federica Galli, Jan M. van Ruitenbeek, and Grégory F. Schneider. Dynamic tunneling junctions at the atomic intersection of two twisted graphene edges. *Nano Letters*, 18(4):2505–2510, 2018. PMID: 29513997.

[41] Jaakko Akola, H. Heiskanen, and Matti Manninen. Edge-dependent selection rules in magic triangular graphene flakes. *Physical Review B*, 77, 04 2008.

[42] Kyoko Nakada, Mitsutaka Fujita, Gene Dresselhaus, and Mildred S Dresselhaus. Edge state in graphene ribbons: Nanometer size effect and edge shape dependence. *Physical Review B*, 54(24):17954, 1996.

[43] Kyoko Nakada, Mitsutaka Fujita, Gene Dresselhaus, and Mildred S. Dresselhaus. Edge state in graphene ribbons: Nanometer size effect and edge shape dependence. *Phys. Rev. B*, 54:17954–17961, Dec 1996.

[44] A. Kretinin, G. L. Yu, R. Jalil, Y. Cao, F. Withers, A. Mishchenko, M. I. Katsnelson, K. S. Novoselov, A. K. Geim, and F. Guinea. Quantum capacitance measurements of electron-hole asymmetry and next-nearest-neighbor hopping in graphene. *Physical Review B*, 88(16), Oct 2013.

[45] Stephanie Reich, J. Maultzsch, Christian Thomsen, and P. Ordejón. Tight-binding description of graphene. *Phys. Rev. B*, 66, 07 2002.

[46] Rolf Landauer. Spatial variation of currents and fields due to localized scatterers in metallic conduction. *IBM Journal of research and development*, 1(3):223–231, 1957.

[47] Rolf Landauer. Electrical resistance of disordered one-dimensional lattices. *Philosophical magazine*, 21(172):863–867, 1970.

[48] M Büttiker. Four-terminal phase-coherent conductance. *Physical review letters*, 57(14):1761, 1986.

[49] S. Datta, H. Ahmad, and M. Pepper. *Electronic Transport in Mesoscopic Systems*. Cambridge Studies in Semiconductor Physi. Cambridge University Press, 1997.

[50] A. MacKinnon. The calculation of transport properties and density of states of disordered solids. *Zeitschrift für Physik B Condensed Matter*, 59(4):385–390, Dec 1985.

[51] D J Thouless and S Kirkpatrick. Conductivity of the disordered linear chain. *Journal of Physics C: Solid State Physics*, 14(3):235–245, jan 1981.

[52] Patrick A. Lee and Daniel S. Fisher. Anderson localization in two dimensions. *Phys. Rev. Lett.*, 47:882–885, Sep 1981.

[53] Christoph W Groth, Michael Wimmer, Anton R Akhmerov, and Xavier Waintal. Kwant: a software package for quantum transport. *New Journal of Physics*, 16(6):063065, jun 2014.

[54] Aaron Bostwick, Taisuke Ohta, Thomas Seyller, K. Horn, and Eli Rotenberg. Experimental determination of the spectral function of graphene, 2006.

[55] G Dresselhaus, Mildred S Dresselhaus, and Riichiro Saito. *Physical properties of carbon nanotubes*. World scientific, 1998.

[56] F. Muñoz Rojas, D. Jacob, J. Fernández-Rossier, and J. J. Palacios. Coherent transport in graphene nanoconstrictions. *Phys. Rev. B*, 74:195417, Nov 2006.

[57] J. C. Slater and G. F. Koster. Simplified lcao method for the periodic potential problem. *Phys. Rev.*, 94:1498–1524, Jun 1954.

[58] F. Muñoz Rojas, J. Fernández-Rossier, and J. J. Palacios. Giant magnetoresistance in ultrasmall graphene based devices. *Phys. Rev. Lett.*, 102:136810, Apr 2009.